Localized Proteotoxic Stress in Mitochondrial Intermembrane Space and Matrix Elicits Sub-compartment Specific Response Pathways Governed by Unique Modulators

Kannan Boosi Narayana Rao[#,1,2], Pratima Pandey[#,1], Rajasri Sarkar[5], Asmita Ghosh[1,2], Shemin Mansuri[3], Mudassar Ali[5], Priyanka Majumder[5], , Arjun Ray[4], Swasti Raychaudhuri[3] and Koyeli Mapa[2,5,$].

1. Proteomics and structural Biology Unit, CSIR-Institute of Genomics and Integrative Biology, Mathura Road, New Delhi 110025, India

2. Academy of Scientific and Innovative Research, CSIR-HRDG, Ghaziabad, Uttar Pradesh 201002, India.

3. CSIR-Centre for Cellular and Molecular Biology, Uppal Road, Hyderabad 500007, India.

4. Centre for Computational Biology, Indraprastha Institute of Information Technology, New Delhi 110020, India

5. Department of Life Sciences, School of Natural Sciences, Shiv Nadar University, Greater Noida, Gautam Buddha Nagar, Uttar Pradesh 201314, India.

# contributed equally to this work

$ Correspondence: koyeli.mapa@snu.edu.in

Abstract

The complex double-membrane architecture of mitochondria is essential for its ATP synthesis function and divides the organelle into two sub-mitochondrial compartments, inter-membrane space (IMS) and matrix. The folding environments of IMS and matrix are significantly different owing to its dissimilar oxido-reductive environments and distinctly divergent protein quality control (PQC) machineries. Here, by inducing proteotoxic stress restricted to IMS or matrix by targeting three different stressor proteins, we show that the cellular response to IMS or matrix-localized misfolding stress is distinct and unique. IMS and matrix stress response pathways are quite effective in combatting stress despite significant stress-induced alteration in mitochondrial phenotypes. IMS misfolding stress leads to specific upregulation of IMS chaperones and components of TOM complex while matrix chaperones and cytosolic PQC components are upregulated during matrix stress. Notably, the amplitude of upregulation of mitochondrial chaperones is not overwhelming. We report that cells respond to mitochondrial stress through an adaptive mechanism by adjourning mitochondrial respiration while upregulating glycolysis as a compensatory pathway. We show that subunits of TOM complex act as specific modulators of IMS-stress response while Vms1 precisely modulates the matrix stress response.

Key words: Mitochondrial Unfolded Protein Response, Proteostasis, Proteotoxic stress, Protein misfolding, Chaperones, Stress Response

Introduction

Mitochondria, the cellular powerhouse, is solely dependent for its biogenesis and function on supply of its constituent proteins as pre-proteins from cytosol. Thus, the organelle continuously import unfolded precursor proteins in its two sub-compartments: mitochondrial matrix (MM) and intermembrane space (IMS). Following their translocation and targeting to the sub-compartments, the precursor proteins are eventually folded and often assembled (into complexes) to their functional forms by the respective chaperone machineries [1-3] . Hence, mitochondrial IMS and matrix are continuously exposed to non-native, precursor proteins which when combined with other sources of proteotoxic stress threaten the health of the organelle. Apart from presence of considerable amount of reactive oxygen species (ROS) generated as a by-product of oxidative phosphorylation within the organelle, recent literature show varied sources of proteotoxic threat to mitochondria like aggregation prone proteins from cytosol which requires clearance by MAGIC pathway [4], mistargeted proteins from neighbouring organelles like endoplasmic reticulum (ER) [5] or higher intra-mitochondrial temperature [6].

To combat such imminent proteotoxic stress, there are designated chaperones and proteases to maintain the folding environment (together known as mitochondrial PQC machinery) in both the sub-mitochondrial compartments, although the nature of folding machineries is markedly different between mitochondrial matrix and IMS [1-3]. When the amount of unfolded, misfolded or unassembled proteins overwhelm the folding capacity of these compartments, mitochondria become stressed and elicit a stress response known as mitochondrial Unfolded Protein Response (mitoUPR) [7, 8]. Over the years, while mitoUPR has been intensively studied, a vast majority of these studies relied on the perturbation of mitochondrial function which do not directly cause protein misfolding [9-11].

Notably, the evidence of mitoUPR originating exclusively from accumulation of misfolded or aggregated proteins in mitochondria is rather rare in literature [12, 13]. The concept of compartmentalized proteostasis within mitochondria is even rarer, given the lack of selectivity of the small-molecule stressors that are routinely used to impart proteotoxic stress. In *C. elegans*, ATFS-1 was shown to be crucial to signal the mitoUPR arising from matrix localized mitochondrial DNA-damage [9, 10]. Thereafter, mammalian transcription factor, ATF5 which is homologous to ATFS-1 has been shown to act similarly in mammalian cells [11]. Although the stress sensing mechanism by ATFS-1 or ATF5 is unique and exciting, the proposed model does not distinguish between the status of IMS and MM. If only one sub-compartment of mitochondria is affected by proteotoxic stress, will it respond in a specific manner? Can cells distinguish intra-mitochondrial location of the misfolded or aggregated proteins?

To address this question and to understand mitochondrial sub-compartment specific stress response, we generated models of mitochondrial IMS and matrix-specific misfolding stress.

By expressing three different stressor proteins harbouring varied misfolding or aggregation-propensities directed to the mitochondrial IMS or matrix, we show that the two sub-mitochondrial compartments respond distinctly and are, at least, partially different in terms of their capacity to handle misfolding stress. Although both scenarios culminate in a global mitochondrial phenotype (severe fragmentation), the stress response signature is distinct and unique between IMS stress and matrix stress. By transcriptome analysis, we demonstrate exclusive upregulation of sub-compartment specific quality control components like Erv1 and small Tim proteins in IMS stress while Hsp60, Tim44 and components of cytosolic PQC in matrix stress. Thus, we have termed such specific responses as IMS-UPR and mito-matrix-UPR respectively. Based on the transcriptome

data, we performed a focused genetic interaction mapping of IMS-UPR and mito-matrix-UPR and show that the two pathways are indeed distinct. By systematic genetic interaction analysis, we found subunits of TOM complex (Tom6, 7 and 22) act as specific modulators of IMS-UPR. In contrast, Vms1, a Ribosome Quality Control (RQC) component which is known to protect mitochondrial proteotoxicity by specifically antagonising CAT-tailing of mitochondrial pre-proteins by Rqc2 [14] and peptidyl-tRNA endonuclease activity[15], plays a central role in mito-matrix UPR. We further show that N-terminal domain of Vms1 containing its VLRF1 (Vms1 like release factor) domain which is indispensable for 60S ribosomal subunit binding and tRNA endonuclease activity [15], to be essential during matrix stress. Kinetic analysis of gene expression revealed differential patterns of mitoPQC, translocase components, cytosolic PQC and various metabolic pathways in IMS and matrix stress. We found substantial downregulation of components of Electron Transport Chain (ETC) at the transcriptome as well as at the proteome level. We show that cells cope with the mitochondrial proteotoxic stress quite efficiently by suspending the mitochondrial functions especially respiration by an adaptive response, particularly during matrix stress and survive by a strategy of altered metabolism. .

Results

Mitochondrial sub-compartments are extremely vulnerable to proteotoxic stress

We employed yeast, *Saccharomyces cerevisiae*, as a model organism to study sub-mitochondrial compartment specific proteotoxic stress response. We took three different exogenous misfolding or aggregation-prone model proteins to induce misfolding stress confined to sub-mitochondrial compartments, inter-membrane space (IMS) and mitochondrial matrix (MM) (Figure 1A). In parallel, we similarly expressed well folded wild type version of the these proteins as controls to specifically dissect the cellular response

elicited exclusively due to misfolding or aggregation and not due to overburdening of mitochondrial protein quality control machineries with foreign proteins. We preferred exogenous model proteins over aggregation prone mutants of endogenous proteins to capture the stress response arising particularly due to misfolding stress and not due to secondary effects of aggregation prone endogenous proteins that might 1) recruit endogenous interaction partners in the aggregated species leading to loss of function and toxicity, 2) co-aggregation of the wild type copy of the protein, where keeping the endogenous copy of the protein becomes essential, 3) exert dominant negative function due to futile interaction with the interaction partners or 4) lead to rewiring of transcription to upregulate a compensatory or parallel pathway due to dominant negative function of the overexpressed mutant protein. IMS and MM-specific targeting of these model proteins was achieved by using the well characterized signal sequence of yeast Cytochrome b2 signal sequence or its truncated version (lacking the 19 amino acid membrane sorting signal also known as Cyb2Δ19) respectively [16, 17]. As one of the stressor protein, we chose slow folding mutant version of *E.coli* Maltose binding protein (MBP) (Figure 1A, left panel) also known as double-mutant MBP (DM-MBP) [18, 19], and due to its slow folding rate, at any point the concentration of the non-native conformation of this protein is higher than that of a fast-folding protein and is expected to induce proteotoxic stress [20]. Indeed when DM-MBP is expressed in ER lumen it elicits ER-UPR but wild type MBP does not induce ER-UPR (Figure 1B) [20]. The second stressor protein used is a mutant form of mouse dihydro-folate reductase (DHFR) which is a misfolded protein and thus gets rapidly degraded in vivo (mutC-DHFR) (Figure 1A, middle panel) [21]. The third stressor protein used, is an artificial amyloid forming protein and hereafter named as protein with misfolded domain (PMD) (Figure 1A, right panel). Previous studies have shown that artificial beta sheet containing model proteins form toxic aggregates and sequester crucial components of cellular protein quality control machinery resulting

toxicity [22]. PMD being much larger in size (~30kDa) like an endogenous yeast protein than these model beta sheet forming proteins, was expected to be toxic. PMD is predicted to contain secondary structural elements of approximately 33.3% of α- helices, 39.3% of ß-strands and 27.4% of random coils (Figure S1A and S1B). Recombinant PMD protein was cloned and purified from *E.coli* (Figure S1C) and was characterised for misfolding and amyloid-forming properties. Indeed, PMD showed very prominent Thioflavin-T (ThT) binding indicating strong amyloid formation (Figure 1C). Another hallmark of misfolding, exposed hydrophobicity, was captured by the blue shift of emission spectra of the fluorescent probe 1,8, ANS(Figure 1D). Remarkably, when PMD was expressed in ER lumen, it elicited ER-UPR like DM-MBP indicating that the artificial amyloid forming protein is correctly recognised as a misfolded protein by the endogenous sensors of ER-UPR and is able to mount stress response (Figure 1B). Wild type (WT) MBP and DHFR were expressed under same promoter as controls for folded protein overexpression. To check the specific response pathways of IMS and MM specific misfolding stress, we targeted same aggregation or misfolding-prone stressor proteins to endoplasmic reticulum (ER), nucleus (N) and cytosol (Cyto) of yeast along with matrix and IMS of mitochondria. All misfolded proteins or the wild type counterparts were expressed from inducible Gal1 promoter with a Cyc terminator for transcription termination (Figure 1E). The whole cassette of Gal1 promoter-signal sequence-protein-Cyc terminator was integrated in the URA3 locus of wild-type yeast strain (YMJ003) (Figure S1D) [23, 24]. Expression of stressor proteins after galactose induction were checked by western blots and no expression was observed without the inducer (galactose) indicating no substantial leaky expression (Figure S1E). Importantly, among all the subcellular compartments, mitochondrial matrix (MM) and IMS exhibited substantial growth defects upon induction of misfolding stress by expressing the amyloid forming protein, PMD, the growth defect was more pronounced upon its expression in matrix (Figure 1F). The slow

folding mutant, DM-MBP imparted slow growth phenotype to IMS although mitochondrial matrix remained unaffected with DM-MBP overexpression. Expression of rapidly degrading misfolded protein mutC-DHFR [21] did not impart any growth defect to either of the mitochondrial sub-compartment (Figure 1G and 1H). With all three stressor proteins, other subcellular compartments tested did not exhibit any visible growth defect (Figure 1F, S1E and S1F). To check, whether the observed slow growth phenotype of IMS and MM strains was due to growth arrest or cell death, we did a recovery experiment. After keeping the cells stressed by continuously expressing stressor proteins for 16 hours, we washed the culture to remove the inducer (galactose) and spotted on the glucose containing media (YPD). As glucose is known to tightly repress the galactose promoter, YPD stops further production of misfolded proteins and cells are expected to recover after withdrawal of stress if cells were growth arrested due to misfolding stress. All strains including the ones that exhibited slow growth phenotype upon expression of stressor proteins in MM and IMS grew similarly when recovered in YPD indicating that the strains with visible phenotype in presence of the inducer (MM-PMD, IMS-PMD and IMS-DMMBP) were mostly growth arrested (Figure S2A). Taken together, we show that mitochondrial sub-compartments, matrix and IMS are extremely vulnerable to proteotoxic stress although these two sub-mitochondrial compartments partially differ in their stress handling capacity as seen by their difference in tolerating the expression of a slow-folding mutant protein, DM-MBP.

Proteotoxic stress in IMS or mitochondrial matrix leads to altered mitochondrial dynamics and functions

Misfolding stress localized to mitochondrial sub-compartments led to significant growth defects, this result hinted at altered mitochondrial function due to protein misfolding. As dysfunctional mitochondria are often associated with alteration in dynamics (often reported to be more fragmented due to increased fission), we checked for any change in mitochondrial

network morphology following misfolding stress. To visualize mitochondria, we targeted ye-GFP (yeast enhanced GFP) to mitochondrial matrix using matrix-specific signal sequence. The control cells (without inducer) showed tubular network of mitochondria with continuous fission and fusion indicating normal mitochondrial dynamics (Figure 2A). In contrast, the strains with visible growth defect (IMS-DM-MBP, IMS-PMD and MM-PMD), showed altered mitochondrial dynamics after induction of proteotoxic stress. Mitochondria were severely fragmented resulting prominent disruption of the tubular network. In some strains (e.g. IMS-PMD,) disruption of tubular mitochondrial network was extremely severe and the fragmented mitochondria were accumulated at one pole of the cells (Figure 2A). Similarly, upon expression PMD protein with a C-terminal GFP tag, we observed significant disruption of mitochondrial network in both matrix and IMS stress (Figure S2B). The cells with overexpressed WT proteins (MBP or DHFR) or mutC-DHFR did not show any alteration in mitochondrial network indicating mere overexpression of any foreign proteins in mitochondrial IMS or matrix do not lead to altered mitochondrial dynamics (Figure S2C) . Hence, the observed fragmentation in strains with visible growth phenotypes was due to misfolding stress. Notably, this altered mitochondrial dynamics upon misfolding stress was recapitulated in mammalian cells. When PMD protein was targeted to HeLa cells using specific targeting signals for mammalian mitochondrial matrix and IMS, we observed severe fragmentation of mitochondrial tubular network in both matrix and IMS stress, more prominently in the matrix stress (Figure 2B). Despite severe fragmentation of mitochondrial network, cell death was negligible in mammalian cells also, as observed in case of yeast cells (Figure S2D).

Next, to check for alteration in mitochondrial functions, the cells were treated with Mitotracker-green, a fluorescent probe that specifically accumulates in normally respiring mitochondria. IMS-PMD and MM-PMD cells were substantially less stained with

Mitotracker green following induction of misfolding stress compared to un-induced cells (Figure S2E). Importantly, MM-PMD cells had far more severe defect in uptake of Mitotracker green probe, after expression of the stressor protein, indicating severe problem in mitochondrial respiration in these cells (Figure S2E). Perturbed mitochondrial respiration was further confirmed by measuring the oxygen consumption rate (OCR). Following induction of misfolding stress, the OCR of IMS-PMD cells were reduced compared to WT cells (Figure 2C). MM-PMD cells showed significant reduction in OCR post misfolding stress as was previously indicated by defective uptake of mitotracker green in these cells (Figure 2C). In summary, we show that misfolding stress due to accumulation of misfolded or aggregated proteins in mitochondrial sub-compartments lead to mitochondrial fragmentation and declined mitochondrial respiration. Interestingly, severe mitochondrial fragmentation, cells can efficiently handle prolonged and sustained mitochondrial stress resulting growth arrest but insignificant cell death from yeast to human cells. This indicates the presence of robust stress response and quality control mechanism for mitochondrial misfolding stress across eukaryotes.

Mitochondrial IMS and matrix responds differently to similar misfolding stresses

To capture the specific cellular response during mitochondrial protein misfolding stress, we did a gene expression analysis by RNA sequencing of the yeast strains expressing different stressor proteins along with its wild-type proteins as controls for exogenous protein overexpression targeted to different sub-cellular compartments (mito-IMS, mito-MM, ER, cytosol, nucleus). We extracted RNA from the yeast strains for transcriptomics study using RNA sequencing after 16 hours of galactose induction keeping un-induced cells and wild type strain as controls (details of strains subjected for RNA sequencing are provided in Supplemental Table S1). We obtained list of differentially upregulated and downregulated genes after induction of proteotoxic stress in different subcellular compartments. To capture

the specific set of genes that are differentially expressed during misfolding stress in a particular subcellular compartment, we calculated the Z-scores of each gene and the genes above or below Z-score 2 were considered as significantly upregulated or downregulated, respectively. We found about 394, 210 and 285 genes to be upregulated specifically upon expression of PMD, DM-MBP and mutC-DHFR respectively, in mitochondrial IMS. On the other hand, upon expression of same proteins in mitochondrial matrix, about 227, 222 and 25 genes were upregulated with expression of PMD, DM-MBP and mutC-DHFR respectively,. Approximately 90 genes were downregulated upon expression of PMD protein IMS while about 15 proteins were downregulated when expressed in matrix. Upon performing a gene interaction network (physical and genetic) analysis of significantly upregulated genes) in mitochondrial IMS and matrix stresses (after expression of PMD), we found completely distinct network of upregulated genes in IMS and matrix stress with the same stressor protein (Figure 3Aand 3B). In case of IMS stress, we found increased expression of components of oxidative folding machinery like *erv1*, small heat shock proteins of mitochondrial IMS like *tim10, tim13*, components of TOM complex like *tom5, tom6, tom7* and components for assembly and chaperoning of Cytochrome C oxidase (*cox14, cox17*) machinery. Apart from these prominent groups, many components of mitochondrial ribosome (components of both large and small subunits) were also found to be upregulated in IMS stress. In contrast, in mitochondrial matrix stress, we found a completely different network of significantly upregulated genes (Figure 3B). In matrix stress, matrix resident chaperones and co-chaperones like *ssc1, hsp60, tim44* were upregulated indicating the stress is specific to matrix. Interestingly, a substantial number of genes involved in cytosolic quality control like *ssa1, ssa2, ssa4, hsp82, hsc82, ydj1, djp1, sis1, cct2* were found to be upregulated specifically in matrix stress (Figure 3B). Importantly, component of Ribosome Quality Control (RQC), *vms1*, which is known to act as a peptidyl-tRNA endonuclease and protect mitochondria by

antagonising the CAT-tailing activity of rqc2 [15, 25] was found to be specifically upregulated in matrix stress (Figure 3B).

Although the Z-score based analysis of gene expression changes across different yeast strains expressing misfolded proteins in different subcellular compartment gave us exclusive signature of transcriptional response of proteotoxic stress specific to IMS or matrix, it portrayed a snapshot of the late response (post 16 hours of induction). To capture the early response and ensuing kinetics of gene expression patterns, we performed RNA sequencing at earlier time points, post expression (after 4 hrs, 8 hrs and 12 hrs of galactose induction) of PMD, DM-MBP and MBP (as control of folded protein) proteins within IMS and matrix. It was important to check the status of genes involved in mitochondrial protein quality control (mitoQC) like chaperones and proteases with mounting of stress response. MitoQC components exhibited interesting kinetics of expression. Canonical molecular chaperones of mitochondrial matrix like *hsp60* or *ssc1* (mitochondrial Hsp70) like were upregulated mostly after 8 hours post induction and then decreased in next 4 hours. Importantly, with expression of folded protein MBP, similar overexpression of *hsp60* or *ssc1* was not observed. This finding reitereated that the mitochondrial stress response is specifically mounted by the presence of misfolded or aggregation prone proteins and not by mere presence of any overexpressed protein within the sub-compartments of the organelle. Notably, both the canonical chaperones were marginally upregulated in response to proteotoxic stress. Other chaperones like *mdj1* and *hsp78* were substantially upregulated with proteotoxic stress in both the sub-compartments showing unique and distinct kinetics (Figure 4A). Notably, these two chaperones were also marginally upregulated with expression of wild type MBP indicative of overburdening of mitoQC machinery irrespective of presence of misfolding stress. The protein levels of the chaperones post 12 hours of induction of misfolding stress were in nice corroboration with the transcriptomics data (Figure 4B). At protein level too,

upregulation of Hsp60 was nominal and upregulation of Ssc1 was only prominent in matrix stress. Remarkably, Hsp60 protein (occasionally Ssc1 also) showed cytosolic accumulation in strains with visible toxicity due to misfolding stress (MM-PMD, IMS-PMD) (Figure 4C).

To further appreciate the specific roles of mitochondrial chaperones during proteotoxic stress, we crossed the chaperone deleted (or depleted) strains with misfolded protein containing strains and checked the genetic interaction of these chaperones with IMS-UPR and mito-matrix-UPR by checking any altered phenotype of crossed strains. Among many such tested, only *ssc1*-knock-down (by crossing with ssc1-damp strain) showed further aggravation of misfolding induced growth phenotypes in DM-MBP/PMD-IMS and PMD-MM strains indicating general importance of Ssc1 during proteotoxic stress in mitochondria irrespective of its location (Figure S3A). Interestingly *mdj1Δ* did not aggravate the growth phenotype further while *ecm10Δ* (matrix hsp70) exhibited alleviation of growth phenotypes in both IMS and MM-PMD strains (Figure S3A). Similarly mitochondrial proteases, m-AAA, i-AAA and lon proteases namely *yta12, yme1, pim1* respectively, did not aggravate the growth phenotype of misfolding induced stress indicating no significant contribution of these proteases, at least individually, in IMS or matrix stress response, during mitochondrial misfolding stress (Figure S3B). With genetic interaction with *cox14Δ* and *cox17Δ* strains (both the genes were specifically upregulated in IMS-UPR), we observed further alleviation or aggravation in IMS or matrix stress but the effects were variable between compartments and with different stressor proteins. Thus their role as specific modulator of IMS-UPR were inconclusive (Figure S3C).

As we observed accumulation of mitochondrial matrix chaperones like Hsp60 or Ssc1, it pointed out a possible block in mitochondrial translocation following mounting of misfolding stress in the organelle. Thus, it was interesting to check the gene expression changes of the translocase components with stress. Upon analysing the expression of components of various

TIM, TOM and MICOS complexes, we observed time dependent transcriptional upregulation of few translocase components of both outer and inner membrane. Components of different translocases like *tom6, tim17, tim23, tim12, mic12* and *mim1* were upregulated in a time-dependent manner. All these subunits were more prominently upregulated in the later part after induction (8-12 hrs) of stress (Figure 4D). In accordance with the transcriptomics data, at protein level, we found several TOM complex components (*tom6, tom40, tom22, tom 70*) to be specifically upregulated in IMS stress after 12 hours of stress with PMD protein (Figure 4E). Notably, there was no prominent transcriptional downregulation of any of the TIM or TOM complex components indicating that translocation block probably happens due to physical block of translocase pores due to decreased translocation rate or clogging of pores with misfolded/aggregated proteins and not due to transcriptional rewiring of translocase components. We postulate that during sustained misfolding stress, due to abrogated mitochondrial respiration and less ATP production, translocation rate across inner membrane declines. This sluggish translocation leads to increased dwelling time of pre-proteins through TOM-TIM translocon pores leading to physical blockage of translocase channels. This ultimately may mimic the cellular scenario as observed for mitochondrial precursor over-accumulation stress (mPOS) [26] especially at the late hours after commencement of misfolding stress.

Cytosolic accumulation of matrix chaperones following longstanding mitochondrial proteotoxic stress precisely indicated mounting of a secondary cellular stress similar to mPOS (mitochondrial precursor over-accumulation stress) or UPRam (Unfolded Protein Response activated by mistargeting of proteins) [26, 27]. To find any evidence for cytosolic stress, we checked the gene expression levels of cytosolic protein quality control (cytoQC) machineries. We observed upregulation of cytosolic chaperones like *ssa4*, *hsp82* and *ssa2* mainly in the late hours (8 hrs and 12 hrs post induction) of induction indicating onset of cytosolic stress

due to accumulation of mitochondrial pre-proteins in the cytosol (Figure S4A). In agreement with the transcriptomic data, at protein level too, many such components of cytoQC like Ssa1, Ssa2, Ssa4, Hsc82, Hsp82, Ydj1, Hsp42, Hsp12, were substantially upregulated (Figure S4B). This data indeed indicated mounting of a secondary cytosolic stress response as a consequence of accumulation of mitochondrial precursor proteins. In contrast to mPOS and UPRam [26, 27], most of the proteasome components were repressed upon misfolding stress in IMS or matrix (Figure S4C).

Taken together our data highlight that mitochondrial IMS or matrix has distinct pattern of stress response to misfolding and are catered by different adaptive mechanisms to handle stress. Although there is specific upregulation of IMS or matrix-resident chaperones due to misfolding stress in the corresponding sub-compartment, the amplitude of chaperone overexpression is not substantial. Interestingly, all mitochondrial chaperones are encoded by nuclear genome and need to be translocated inside the organelle which becomes challenging during overwhelming stress leading to translocation block. In consequence, cellular adaptive response to mitochondrial misfolding stress has evolved in a unique manner and does not prominently rely on upregulation of mitochondrial chaperones or proteases, in contrast to ER-UPR or cytosolic heat shock response (HSR).

Mitochondrial respiration is abrogated as an adaptive cellular response to misfolding stress

While analysing the transcriptomics data, one of the most striking finding was severe transcriptional repression of majority of components of mitochondrial Electron Transport Chain (ETC) during matrix stress and IMS stress (Figure 5A). While the transcriptional repression was substantial for majority of the components of complex III, V and half of the components of complex IV in matrix stress, the repression was less for complex III and V

components in IMS stress (Figure 5A). Interestingly, misfolding stress in IMS by two different stressor proteins of distinct (mis)folding properties showed different patterns of expression of some components of ETC (e.g. Qcr7/8/9 of complex III and atp15/17/4, Tim11 of complex V) indicating stressor-protein specific transcriptional stress response in the same mitochondrial sub-compartment (Figure 5A). Importantly components of complex I, *nde1/nde2* or the subunits which are encoded in the mitochondrial genome like COB (component of complex III), *atp6, atp8, oli1* (components of complex V) were not repressed suggesting that the primary route of response to mitochondrial stress is through the nuclear genome. Downregulation of most of the respiratory chain complex (RCC) components were nicely recapitulated at the proteome level also (Figure S5A). Surprisingly, complex 2 components (Sdh1, Sdh2, Sdh3 and Sdh4) were found to be upregulated at protein level during matrix stress, the exact cause of this upregulation of complex 2 subunits remains to be explored.

To check whether abrogation of mitochondrial respiration by downregulation of OX-PHOS components is an adaptive response to mitochondrial misfolding stress, we forced the cells to undergo mitochondrial respiration in non-fermentable media in presence of misfolding stress. The growth phenotype due to misfolding stress deteriorated further in non-fermentable media more prominently in matrix stress (glycerol) indicating adverse effect of forceful mitochondrial respiration during proteotoxic stress in the organelle (Figure S4D). Furthermore, we checked the effect of anti-oxidants or ROS (Reactive Oxygen species) scavengers which are known to improve the mitochondrial respiration and are promising therapeutic agents in pathologies associated with mitochondrial dysfunctions [28]. Indeed, mitochondrial respiration in presence of ascorbate, a known anti-oxidant and a ROS scavenger, improves the OCR of the stressed cells (Figure 5B and Figure S5B). Remarkably, presence of ascorbate or another ROS scavenger N-acetyl cysteine (NAC) during

mitochondrial misfolding stress proved detrimental for cellular health as growth of stressed cells deteriorated further in presence of these compounds (Figure 5C). Thus, our data demonstrate that antioxidants may not be universally beneficial for all types of mitochondrial pathologies, especially those associated with mitochondrial misfolding stress. Together, we show that shutdown of mitochondrial respiration is implemented by cells as an adaptive response to misfolding stress in the organelle and forcing cells to continue respiration during stress proves damaging for the cell and the organism.

We have shown initially that cells remain viable even after sustained misfolding stress and grow like non-stressed cells after withdrawal of the stress (Figure S2A). Thus, it can be presumed that to circumvent the stress situation, cells adopt alternate energy metabolism strategy while maintaining suspended mitochondrial respiration. Indeed, when we analysed the transcriptome and proteome data, we observed substantial upregulation of genes involved in glycolysis and the upregulation was more prominently observed during the matrix stress (Figure S5C, S5D and Figure 5D). This finding aligns well with the respiratory status of mitochondria during matrix stress demanding activation of alternate energy metabolism pathways (Figure 2C). This also suggests that yeast cells bypass the mitochondrial misfolding stress by shifting the metabolism towards glycolysis. Concordantly, TCA cycle components were found to be downregulated at the transcriptome as well as proteome level (Figure S5E, S5F and Figure 5D).

Taken together, we report that misfolding stress in mitochondria remodel the nuclear transcriptome to repress mitochondrial respiration and TCA cycle while activating alternate energy producing pathways like glycolysis. This rewiring is critical in maintaining cellular homeostasis during mitochondrial stress.

Sub-compartment specific stress response modulators of mitochondrial IMS and matrix misfolding stress

First set of transcriptome analysis based on Z-scores across various yeast strains harbouring proteotoxic stress in different subcellular locations, enabled us to depict stress response patterns exclusive of IMS or matrix misfolding stress (Figure 3). Upregulation of components of TOM complex were specifically evident upon IMS stress (Figure 3A) which was further validated at the protein level (Figure 4E). This result prompted us to do a systematic genetic interaction with deletion strains of TOM complex components. Subsequently, we found that deletion of small TOM components like Tom6, Tom7 and Tom receptors like Tom22 further aggravate the severity of growth phenotypes of IMS stress (Figure 6A and 6B). In contrast, other outer mitochondrial membrane protein like porin (por1), does not affect the IMS-UPR. Notably, the effect of deletion of these TOM components is exclusive for IMS stress and does not affect the phenotype of matrix stress (Figure S6A and S6B). This clearly indicate the importance of TOM complex in the IMS misfolding stress. Recently, identification of various stress response pathways like mitochondrial compromised protein import response (mitoCPR)[29], mitochondrial translocase associated degradation (mitoTAD)[30] have shown the importance of components TOM complex like Tom70 in recruiting various proteases like Msp1, Ubx2 during stress which subsequently help to restore the cellular homeostasis [29-31]. Our model of IMS misfolding stress (imparted by bipartite signal sequence containing stressor proteins) would mimic the cellular response like mitoCPR especially during long standing chronic stress. Our data show that not only Tom70 but other TOM complex components like small TOM proteins like Tom6, Tom7 and receptors components proteins like Tom22 also play crucial role in IMS misfolding stress response.

Interestingly, the TOM complex components which are crucial for IMS-UPR, do not regulate the mito-matrix-UPR (Figure S6A and S6B).

On the contrary, upon systematic genetic interactions with deletion strains of matrix stress specific upregulated genes, we found presence of Vms1 to be critical for mito-matrix-UPR. Vms1 is known as a key component of Mitochondria Associated Degradation (MAD) pathway[32-34] and an important player of Ribosome Quality Control of stalled ribosomes [14, 15, 25, 35, 36]. Deletion of *vms1* in the matrix and IMS misfolding strains, revealed its explicit role in matrix misfolding stress (Figure 6C). The growth phenotype due to matrix stress worsened in absence of *vms1*, while similar effect was not apparent in IMS stress (Figure 6D). To check the localization of Vms1 during matrix misfolding stress, we expressed Vms1-tagged to C-terminal GFP under its native promoter in the MM-PMD-*vms1*Δ cells. We found two bands for Vms1-GFP of ~95kDa and ~65kDa (molecular weight calculated without GFP-tag), bands of similar size were also observed with Flag-tagged Vms1 (data not shown). Both forms of the protein were present in the whole cell extract as well in the cytosolic fraction although only the higher form (~95kDa) was detected in the mitochondrial fraction in minor amount (Figure 6E). In agreement with the western blot result, Vms1-GFP was found to be majorly localized in cytosol and no significant co-localization was observed with MitoTracker Red dye by fluorescence microscopy (Figure S6C). This data indicates that extra-mitochondrial functions of Vms1 during matrix stress is crucial for mito-matrix-UPR. From this result we speculated that the CAT-tailed mitochondrial pre-proteins accumulate and aggregate in absence of antagonistic effect of Vms1 on Rqc2's CAT-tailing activity which pose further problem in already stressed mitochondria [14]. To test this possibility, we deleted *rqc2*, *ltn1* in MM-PMD strain, and deletion of these RQC components alleviated the phenotype of MM-PMD in contrast to more severe phenotype with *vms1*Δ (Figure 6F and

Figure S6D). This data indeed show that a stringent -RQC by controlled CAT-tailing of mitochondrial precursor proteins with antagonistic activity of Rqc2 and Vms1 is essential during matrix misfolding stress. Additionally, we deleted the MAD component *doa1* in MM-PMD strain. Deletion of *doa1* alleviated the phenotype of MM-PMD. Recently it was shown that *doa1* is a key player of MAD-dependent degradation of not only mitochondrial outer membrane proteins but also proteins of matrix and inner membrane [37]. Importantly, among the matrix MAD targets, matrix chaperones (Hsp60, Ssc1) and protease (Pim1) were detected. We speculate that increased steady state levels of these mitoQC components especially chaperones like Ssc1, in *doa1* deleted cells may become beneficial during matrix stress.

As Vms1 was previously implicated in mitochondrial respiration and we found mitochondrial respiration is suspended as an adaptive response to matrix stress, it was interesting to check the effect of absence of Vms1 on mitochondrial respiration during stress. We henceforth measured the OCR of vms1Δ cells which showed comparatively less OCR in vms1Δ cells than the non-deleted strain in absence of misfolding stress (un-induced MM-PMD-vms1Δ cells and MM-PMD cells) (Figure S6E). Surprisingly OCR was increased in induced MM-PMD- vms1Δ cells compared to MM-PMD cells (Figure S6E). This result indicates that Vms1 play an important role in cellular adaptive response of limiting the mitochondrial respiration during misfolding stress. This role of Vms1 corroborates well with the observed growth phenotype aggravation of MM-PMD-*vms1*Δ cells during stress (Figure 6C).

To identify domains of Vms1 that are crucial during misfolding stress, we transformed different truncation mutants of Vms1 in *vms1Δ* cells. Along with full-length Vms1 (Vms1-FL) as control, only the N-terminal domain of Vms1 (1-417aa, named as Vms1-NTD), Vms1 with deletion of VIM (VCP Interacting Motif) domain (named as

Vms1ΔVIM, 1-616 aa) and Vms1 with truncation of N-terminal domain (named as Vms1ΔN, 418-632 aa) were expressed in the background of MM-PMD- *vms1Δ* strain (Figure 6G). Vms1-NTD and Vms1ΔVIM complemented the *vms1Δ* phenotype like full-length Vms1, although Vms1ΔN could not complement the phenotype of vms1Δ during matrix stress (Figure 6H). The lack of complementation of *vms1Δ* phenotype by Vms1ΔN was exclusive for matrix stress and was not observed in IMS stress (Figure S6F). This data indicated that N-terminal domain (1-417aa) of Vms1 containing its VLRF1 domain is critical for its RQC function for its 60S subunit binding and peptidyl-tRNA endonuclease activity [15] and the domain has a crucial role during mitochondrial matrix misfolding stress.

Thereafter, we compared the effect of N-terminal truncation of Vms1 on mitochondrial respiration by expressing Vms1 or Vms1ΔN by measuring the OCR (Figure S6G). Interestingly, we found higher OCR of MM-PMD-vms1Δ cells expressing Vms1ΔN compared to the cells expressing full length Vms1. This data indicated that the Vms1 play crucial role in keeping a check on mitochondrial respiration during matrix misfolding stress through its N-terminal domain (1-417 amino acids). As the N-terminal domain has been recently shown to harbour peptidyl-tRNA hydrolase/endonuclease activity in its VLRF1 domain [15, 25, 35], we speculate that these activities of the protein is important for suspending the mitochondrial respiration as an adaptive response to matrix stress.

Thus, we show that matrix misfolding stress when combined with absence or non-functional Vms1, becomes severely detrimental probably due to accumulation and aggregation of unchecked CAT-tailed mitochondrial pre-proteins which cause additional problems in already stressed mitochondria. We speculate that among these proteins, some CAT-tailed pre-proteins might be functional and those functional OX-PHOS components

which end up in mitochondria continue respiration which becomes further challenging to be handled by cells.

Discussion

In recent years, understanding mitochondrial proteostasis and communication of mitochondria with outside during various stresses, have gained much attention. Extensive research in the related fields have yielded the discovery of novel stress response pathways like mitoUPR, MAGIC[4], mPOS[27], UPRam[26], mitoCPR[29, 38], mitoTAD[30], MISTERMINATE [39, 40] which have shed lights on extremely specialized and unique cellular pathways to thwart mitochondrial or mitochondria-associated stresses. In the current study, we have moved a step further beyond generalized mitochondrial stress and have asked whether cellular response would be exclusive to localized stresses within mitochondrial sub-compartments. Indeed, we show that cells can sense localized intra-mitochondrial misfolding stress which in turn is reflected as distinct stress response for mitochondrial IMS or matrix. Importantly, we show that mere overexpression of folded proteins does not noticeably alter mitochondrial dynamics or the organelle function and cells do not elicit canonical stress response after overexpression of folded proteins. Interestingly, none of the canonical mitochondrial chaperones are overwhelmingly expressed post misfolding stress either at RNA or protein level. We speculate that cells have evolved rather unconventional stress response mechanism for this unique organelle. As the mitoQC components are exclusively encoded by the nuclear genome, it will be a challenging task to import the chaperones and proteases by an energy-expending process, especially those belonging to mitochondrial matrix, to mitigate the stress. Furthermore, suspended mitochondrial respiration during misfolding stress would lead to inefficient translocation of mitoQC components, so producing these quality control components

become a futile exercise. In such a scenario, mitochondria need to circumvent the stress situation and restore homeostasis by not relying on its own quality control machinery, rather it has evolved non-canonical pathways to handle misfolding stress. We show that components of TOM complex are crucial during IMS stress. We speculate that a longstanding IMS stress would mimic responses similar to mitoCPR involving not only Tom70 but also other TOM subunits like Tom6, Tom7 and Tom22 (Figure 7) and would bring back the homeostasis possibly by recruiting the specific proteases like Msp1, Ubx2 to clear the misfolded proteins from clogged TOM complex and IMS (Figure 7, upper panel). Import across the outer membrane being energy-independent, outer mitochondrial membrane associated quality control is easy to implement, at least for proteotoxic stress in IMS. In contrast, similar stress in mitochondrial matrix largely depends on cytosolic quality control and mitochondria-associated Ribosome Quality Control (mito-RQC). We show that RQC component Vms1 (Figure 7, lower panel), through its N-terminal domain, play a crucial role to limit the mitochondrial respiration which is suspended as an adaptive response during mitochondrial misfolding stress. We found many components of cytosolic quality control are upregulated during long standing mitochondrial stress (both in matrix and IMS) indicating important role of cytosolic quality control machinery in protecting the stressed organelle. Our current findings and previous works describing stress response pathways like mitoCPR, mitoUPR, MAGIC, mitoTAD etc., altogether indicate a meticulous symbiosis between mitochondria and cytosol, especially under situations of protein misfolding stress within and around the organelle. In effect, we see IMS-UPR and mito-matrix-UPR successfully tackle the stress with no significant cell death despite severe mitochondrial fragmentation and abrogated respiration, rather cell growth and mitochondrial dynamics are restored efficiently after withdrawal of stress. This efficient stress handling capacity of mitochondria is observed from unicellular

eukaryote yeast to complex human cells. Whether specific modulators of IMS-UPR (specific components of TOM complex) and mito-matrix-UPR (Vms1) as found in yeast are conserved across eukaryotes, remains to be checked.

Acknowledgements

We thank Dr. Dejana Mokranjac for sharing the Cyb2-DHFR plasmid. We thank Prof. Jared Rutter for sharing the Vms1 and Vms1 truncation mutant plasmids. We thank Dr. Claes Andreasson for sharing the mutC-DHFR plasmid. We thank Dr. Kausik Chakraborty for sharing the YMJ003 yeast strain and R script for RNA sequencing data analysis. We thank Aseem Chaphalkar for the UPRE-GFP FACS measurement. KM and SR acknowledge the funding from Department of Biotechnology (DBT), Government of India for grant in Basic Research in Modern Biology, grant number (BT/PR28386/BRB/10/1671/2018). KM also acknowledges partial funding support from Science and Engineering Research Board (SERB), Government of India, for Core Research Grant (SERB/CRG/2019/006281) and SNU core funding. SR is a DBT-Ramalingaswami Fellow (BT/RLF/Re-entry/43/2012). Mr. K Ranjith Kumar at the Proteomics facility at CSIR-CCMB is acknowledged for mass spectrometry experiments. We acknowledge Gopal Gunanathan Jayaraj for help in RNAseq library preparation,preliminary data analysis and for critical comments on the manuscript. We acknowledge core Imaging facility and central Instrumentation facility of CSIR-IGIB. Mr. Manish Kumar at CSIR-IGIB and SNU imaging facility is acknowledged for help is imaging data analysis. We thank Monika Verma, Nishtha Bhargava and Kanika Verma for critical comments on the manuscript. KBN acknowledges CSIR SRF grant [31/43(350)/2017-EMR-I], PP acknowledges the DST WosA grant (SR/WOS-A/LS-99/2014). PM acknowledges SERB NPDF grant (SERB/F/4161/2018-2019). RS acknowledges ICMR SRF grant (2019-6710/CMB/BMS) and SNU PhD fellowship. MA acknowledges SNU PhD fellowship.

Author Contribution

The work was conceived by KM. All yeast strains were generated by KBN and PP. Yeast experiments were done by KBN, PP and RS. Biophysical characterization of PMD protein was done by KM. RNA sequencing library preparation and sequencing run was performed by KBN, AG. Data analysis was done by AG and KM. Samples for proteomics were made by RS, proteomics run and data analysis were done by SM and SR. PMD protein simulation and secondary structural analysis were done by AR. Mammalian cell experiments were done by MA and PM. KM analysed the data and wrote the manuscript.

References

1. Priesnitz, C., Pfanner, N. & Becker, T. Studying protein import into mitochondria. *Methods Cell Biol* **155**, 45-79 (2020).
2. Neupert, W. & Herrmann, J.M. Translocation of proteins into mitochondria. *Annu Rev Biochem* **76**, 723-749 (2007).
3. Backes, S. & Herrmann, J.M. Protein Translocation into the Intermembrane Space and Matrix of Mitochondria: Mechanisms and Driving Forces. *Front Mol Biosci* **4**, 83 (2017).
4. Ruan, L. *et al.* Cytosolic proteostasis through importing of misfolded proteins into mitochondria. *Nature* **543**, 443-446 (2017).
5. Costa, E.A., Subramanian, K., Nunnari, J. & Weissman, J.S. Defining the physiological role of SRP in protein-targeting efficiency and specificity. *Science* **359**, 689-692 (2018).
6. Chretien, D. *et al.* Mitochondria are physiologically maintained at close to 50 degrees C. *PLoS Biol* **16**, e2003992 (2018).
7. Haynes, C.M. & Ron, D. The mitochondrial UPR - protecting organelle protein homeostasis. *J Cell Sci* **123**, 3849-3855 (2010).
8. Anderson, N.S. & Haynes, C.M. Folding the Mitochondrial UPR into the Integrated Stress Response. *Trends Cell Biol* **30**, 428-439 (2020).
9. Nargund, A.M., Pellegrino, M.W., Fiorese, C.J., Baker, B.M. & Haynes, C.M. Mitochondrial import efficiency of ATFS-1 regulates mitochondrial UPR activation. *Science* **337**, 587-590 (2012).
10. Nargund, A.M., Fiorese, C.J., Pellegrino, M.W., Deng, P. & Haynes, C.M. Mitochondrial and nuclear accumulation of the transcription factor ATFS-1 promotes OXPHOS recovery during the UPR(mt). *Mol Cell* **58**, 123-133 (2015).
11. Fiorese, C.J. *et al.* The Transcription Factor ATF5 Mediates a Mammalian Mitochondrial UPR. *Curr Biol* **26**, 2037-2043 (2016).
12. Zhao, Q. *et al.* A mitochondrial specific stress response in mammalian cells. *EMBO J* **21**, 4411-4419 (2002).

13. Radke, S. *et al.* Mitochondrial protein quality control by the proteasome involves ubiquitination and the protease Omi. *J Biol Chem* **283**, 12681-12685 (2008).
14. Izawa, T., Park, S.H., Zhao, L., Hartl, F.U. & Neupert, W. Cytosolic Protein Vms1 Links Ribosome Quality Control to Mitochondrial and Cellular Homeostasis. *Cell* **171**, 890-903 e818 (2017).
15. Su, T. *et al.* Structure and function of Vms1 and Arb1 in RQC and mitochondrial proteome homeostasis. *Nature* **570**, 538-542 (2019).
16. Popov-Celeketic, D., Mapa, K., Neupert, W. & Mokranjac, D. Active remodelling of the TIM23 complex during translocation of preproteins into mitochondria. *EMBO J* **27**, 1469-1480 (2008).
17. Geissler, A. *et al.* Membrane potential-driven protein import into mitochondria. The sorting sequence of cytochrome b(2) modulates the deltapsi-dependence of translocation of the matrix-targeting sequence. *Mol Biol Cell* **11**, 3977-3991 (2000).
18. Wang, J.D., Michelitsch, M.D. & Weissman, J.S. GroEL-GroES-mediated protein folding requires an intact central cavity. *Proc Natl Acad Sci U S A* **95**, 12163-12168 (1998).
19. Mapa, K., Tiwari, S., Kumar, V., Jayaraj, G.G. & Maiti, S. Information encoded in non-native states drives substrate-chaperone pairing. *Structure* **20**, 1562-1573 (2012).
20. Bandyopadhyay, A. *et al.* Chemical chaperones assist intracellular folding to buffer mutational variations. *Nat Chem Biol* **8**, 238-245 (2012).
21. Gowda, N.K., Kandasamy, G., Froehlich, M.S., Dohmen, R.J. & Andreasson, C. Hsp70 nucleotide exchange factor Fes1 is essential for ubiquitin-dependent degradation of misfolded cytosolic proteins. *Proc Natl Acad Sci U S A* **110**, 5975-5980 (2013).
22. Olzscha, H. *et al.* Amyloid-like aggregates sequester numerous metastable proteins with essential cellular functions. *Cell* **144**, 67-78 (2011).
23. Maity, S. *et al.* Oxidative Homeostasis Regulates the Response to Reductive Endoplasmic Reticulum Stress through Translation Control. *Cell Rep* **16**, 851-865 (2016).
24. Jonikas, M.C. *et al.* Comprehensive characterization of genes required for protein folding in the endoplasmic reticulum. *Science* **323**, 1693-1697 (2009).
25. Zurita Rendon, O. *et al.* Vms1p is a release factor for the ribosome-associated quality control complex. *Nat Commun* **9**, 2197 (2018).
26. Wrobel, L. *et al.* Mistargeted mitochondrial proteins activate a proteostatic response in the cytosol. *Nature* **524**, 485-488 (2015).
27. Wang, X. & Chen, X.J. A cytosolic network suppressing mitochondria-mediated proteostatic stress and cell death. *Nature* **524**, 481-484 (2015).
28. Fiorani, M., Guidarelli, A. & Cantoni, O. Mitochondrial reactive oxygen species: the effects of mitochondrial ascorbic acid vs untargeted and mitochondria-targeted antioxidants. *Int J Radiat Biol*, 1-8 (2020).
29. Weidberg, H. & Amon, A. MitoCPR-A surveillance pathway that protects mitochondria in response to protein import stress. *Science* **360** (2018).
30. Martensson, C.U. *et al.* Mitochondrial protein translocation-associated degradation. *Nature* **569**, 679-683 (2019).
31. Basch, M. *et al.* Msp1 cooperates with the proteasome for extraction of arrested mitochondrial import intermediates. *Mol Biol Cell* **31**, 753-767 (2020).
32. Lamech, L. & Haynes, C.M. Mitochondrial Sterol Oxidation Marks the Spot. *Mol Cell* **68**, 641-642 (2017).

33. Heo, J.M., Nielson, J.R., Dephoure, N., Gygi, S.P. & Rutter, J. Intramolecular interactions control Vms1 translocation to damaged mitochondria. *Mol Biol Cell* **24**, 1263-1273 (2013).
34. Heo, J.M. *et al.* A stress-responsive system for mitochondrial protein degradation. *Mol Cell* **40**, 465-480 (2010).
35. Verma, R. *et al.* Vms1 and ANKZF1 peptidyl-tRNA hydrolases release nascent chains from stalled ribosomes. *Nature* **557**, 446-451 (2018).
36. Kreft, S.G. & Deuerling, E. Vms1: A Cytosolic CAT-Tailing Antagonist to Protect Mitochondria. *Trends Cell Biol* **28**, 3-5 (2018).
37. Liao, P.C., Wolken, D.M.A., Serrano, E., Srivastava, P. & Pon, L.A. Mitochondria-Associated Degradation Pathway (MAD) Function beyond the Outer Membrane. *Cell Rep* **32**, 107902 (2020).
38. Desai, R. & Campanella, M. MitoCPR: Meticulous Monitoring of Mitochondrial Proteostasis. *Mol Cell* **71**, 8-9 (2018).
39. Wu, Z. *et al.* MISTERMINATE Mechanistically Links Mitochondrial Dysfunction with Proteostasis Failure. *Mol Cell* **75**, 835-848 e838 (2019).
40. Lu, B. & Guo, S. Mechanisms Linking Mitochondrial Dysfunction and Proteostasis Failure. *Trends Cell Biol* **30**, 317-328 (2020).
41. Shannon, P. *et al.* Cytoscape: a software environment for integrated models of biomolecular interaction networks. *Genome Res* **13**, 2498-2504 (2003).
42. Baryshnikova, A. *et al.* Synthetic genetic array (SGA) analysis in Saccharomyces cerevisiae and Schizosaccharomyces pombe. *Methods Enzymol* **470**, 145-179 (2010).
43. Newman, L.E., Schiavon, C. & Kahn, R.A. Plasmids for variable expression of proteins targeted to the mitochondrial matrix or intermembrane space. *Cell Logist* **6**, e1247939 (2016).
44. Valente, A.J., Maddalena, L.A., Robb, E.L., Moradi, F. & Stuart, J.A. A simple ImageJ macro tool for analyzing mitochondrial network morphology in mammalian cell culture. *Acta Histochem* **119**, 315-326 (2017).
45. Ghosh, A. *et al.* Cellular responses to proteostasis perturbations reveal non-optimal feedback in chaperone networks. *Cell Mol Life Sci* **76**, 1605-1621 (2019).
46. Shevchenko, A., Wilm, M., Vorm, O. & Mann, M. Mass spectrometric sequencing of proteins silver-stained polyacrylamide gels. *Anal Chem* **68**, 850-858 (1996).
47. Rappsilber, J., Ishihama, Y. & Mann, M. Stop and go extraction tips for matrix-assisted laser desorption/ionization, nanoelectrospray, and LC/MS sample pretreatment in proteomics. *Anal Chem* **75**, 663-670 (2003).
48. Cox, J. & Mann, M. MaxQuant enables high peptide identification rates, individualized p.p.b.-range mass accuracies and proteome-wide protein quantification. *Nat Biotechnol* **26**, 1367-1372 (2008).
49. Tyanova, S. *et al.* The Perseus computational platform for comprehensive analysis of (prote)omics data. *Nat Methods* **13**, 731-740 (2016).

Figure legends

Figure 1: Mitochondrial sub-compartments, IMS and matrix are extremely vulnerable to proteotoxic stress.

A. Left, middle and right panels are depicting ribbon structure of *E.coli* MBP (PDB ID 1OMP, mutations of DMMBP, V8G and Y283D are shown as space fill), mouse DHFR (PDB ID 3D80, mutations of mutC-DHFR, T39A, E173D, are shown as space fill), and schematic picture of amyloid forming PMD protein respectively. **B**. Bar diagram showing the UPRE-GFP level as a surrogate for induction of ER-UPR by expression of ER-targeted stressor proteins DMMBP and PMD proteins. Wt MBP is expressed in ER lumen as a control. A schematic picture of the UPRE-GFP reporter with mCherry under constitutive Tef2 promoter as control of cellular transcription/translation is shown as inset. Error bars represent standard deviation between repeats (n=3). **C**. Fluorescence emission spectra of free Thioflavin T (ThT) and ThT bound to purified PMD protein in two different concentrations are shown. **D**. Fluorescence emission spectra of 1,8 bis-ANS in buffer and bound to purified PMD protein shown. **E.** Schematic representation of DNA cassettes used for expression of stressor proteins specifically targeted to different sub-cellular compartments. "SS" indicates Signal Sequences for targeting to different subcellular compartments like endoplasmic reticulum, mitochondrial IMS, mitochondrial matrix and nucleus. Gal1p and Cyc term indicates Gal1 promoter and Cyc terminator respectively. **F**. Drop-dilution assay of different yeast strains expressing the amyloid forming PMD protein in different subcellular compartments including mitochondrial IMS and matrix are shown. In the YPR (Yeast extract-Peptone-Raffinose) with inducer (1% galactose), slow growth phenotype in IMS-PMD and MM-PMD strains are visible compared to the control plate without inducer (YPR). "*" and "**" indicates spots with visible growth phenotype in case of IMS-PMD and MM-PMD strains respectively. The time mentioned in hours at the upper right corner of the panel indicates the time of incubation of the spotted plates at 30°C before taking pictures. **G-H**. Drop-dilution assay as described in panel F is shown for strains containing mitochondrial IMS and matrix targeted DMMBP (with wt MBP as control) (panel **G**) and mutCDHFR (with wt DHFR as control) (panel **H**). "*" and "**" indicates spots with visible growth phenotype in case of IMS-PMD or IMS-DMMBP and MM-PMD strains respectively. The time mentioned in hours at the upper right corner of the panel indicates the time of incubation of the spotted plates at 30°C before taking pictures.

Figure 2: Proteotoxic stress in mitochondrial sub-compartments, IMS and matrix leads to alteration in mitochondrial forms and functions.

A. Fluorescence confocal microscopy of yeast cells showing green fluorescent mitochondria expressing mitochondria targeted yeGFP in the MM-DMMBP (Left panel), IMS-DMMBP

(Middle panel) and IMS-PMD strains (Right panel) in absence and presence of galactose induction of stressor proteins in respective mitochondrial sub-compartments. **B**. Left panel: Fluorescence confocal microscopy of HeLa cells showing fluorescent mitochondria constitutively expressing matrix and IMS targeted PMD protein tagged with C-terminal EGFP. To show the mitochondria specific localization of PMD-GFP, co-localization with MitoTracker Deep Red dye have been shown. Right panel: Bar plot showing the mean branch length of mitochondria in control cells (cells expressing EGFP in matrix or IMS) and cells expressing PMD proteins specifically in matrix or IMS. Error bars represent standard deviation among different mitochondrial segments (n=15). Statistical analysis was done by Student's t-test. P value **C**. Oxygen consumption rate (OCR) of Wt (upper panel), IMS-PMD (lower left) and MM-PMD (lower right) strains of yeast are shown in absence and presence of galactose induction.

Figure 3: Transcriptional response of mitochondrial IMS and matrix misfolding stress are distinctly different.

A. Network (both genetic and physical) of genes (specifically upregulated in IMS-UPR post 16 hours of galactose induction to express PMD protein in IMS). Genes with expression level above Z-score 2 were taken for making the network in Cytoscape (version 3.8.0) [41]. The size of the nodes indicate closeness centrality in a scale of 0 to 0.46 and the colours indicate betweenness centrality of the nodes in the network in a scale of 0 (blue) to 0.06 (pink). IMS-resident oxidative folding machinery components are shown with black arrows, components of TOM complex are shown with red arrows. **B**. Network (both genetic and physical) of mito-matrix-UPR upregulated genes (specifically upregulated in mito-matrix-UPR post 16 hours of galactose induction to express PMD protein in matrix) are shown, the genetic network was constructed as described in panel A. Subnetwork of mitochondrial matrix chaperones are highlighted with red dashed box, subnetwork of cytosolic quality control components are highlighted with blue dashed box and Vms1 has been shown with a red arrow.

Figure 4: The amplitude of overexpression of mitochondrial quality control components (mitoQC) is not substantial while canonical chaperones are accumulated in cytosol in response to IMS or matrix misfolding stress

A. Gene expression changes mitoQC components of yeast strains with IMS and matrix (MM) misfolding stress due to overexpression of stressor proteins post 4 hrs, 8 hrs and 12 hrs

of galactose induction are depicted as heatmap. Wt MBP has been kept as control of overexpression of a folded protein in the respective compartments. The fold changes of gene expressions in log2 scale in comparison to 0 time point of each strain have been plotted as heat map. **B**. Heatmap of Z-scores depicting protein-abundance of mitochondrial chaperones and proteases after 12 hours of expression of PMD protein in matrix (MM) or IMS (n=2). **C**. Western blot of mitochondrial matrix chaperones, Hsp60 and Ssc1 showing cytosolic accumulation of chaperones after 12 hours of misfolding stress by PMD protein in mitochondrial matrix and IMS. Lanes without galactose are shown as controls. **D.** Gene expression changes of translocase (TOM, TIM, OXA and MICOS complexes) components of yeast strains with IMS and matrix (MM) misfolding stress are shown as heat map as described in panel A. **E**. Heatmap of Z-scores depicting protein-abundance of mitochondrial translocases after 12 hours of expression of PMD protein in matrix (MM) or IMS (n=2).

Figure 5: Mitochondrial respiration is abrogated as an adaptive response to misfolding stress especially during matrix misfolding stress.

A. Gene expression changes of components of respiratory chain complex (or components of OX-PHOS complexes) of yeast strains with IMS and matrix (MM) misfolding stress due to overexpression of stressor proteins post 4 hrs, 8 hrs and 12 hrs of galactose induction are shown as heatmap. Wt MBP has been kept as control of overexpression of a folded protein in the respective compartments. The fold changes of gene expressions in log2 scale in comparison to 0 time point of each strain have been plotted as heat map. **B**. Oxygen consumption rate (OCR) of IMS-PMD (upper panel) and MM-PMD (lower panel) strains with and without misfolding stress and in presence and absence of antioxidant, ascorbate is plotted. **C**. Drop-dilution assay as of yeast strains containing mitochondrial IMS and matrix targeted stressor proteins DMMBP and PMD (with wt MBP as control) in presence of inducer and inducer plus antioxidants, ascorbate (upper panel) and N-acetyl cysteine (NAC) (lower panel). “*” and “**” indicates spots with visible growth phenotype in case of IMS-PMD or IMS-DMMBP and MM-PMD strains respectively as shown in Figure 1F. “*+” and “**+” indicates spots with further aggravation of growth phenotype in presence of ascorbate or NAC in IMS-PMD/IMS-DMMBP and MM-PMD respectively. Time mentioned in hours at the upper right corner of the panel indicates the time of incubation of the spotted plates at 30°C before taking pictures. **D**. Schematic representation of glycolysis and TCA cycle and

genes involved in each step. Changes of these enzymes both at the transcriptome and proteome level during the matrix stress (MM-PMD strain at 12 hours post galactose induction) have been represented with colour coding.

Figure 6: Components of TOM complex and Vms1 act as specific modulators of IMS-UPR and mito-matrix-UPR respectively.

A-B. Drop-dilution assay as of yeast strains containing single deletion of different components of TOM complex containing mitochondrial IMS targeted stressor protein PMD in presence and absence of the inducer. "*"indicates spots with visible growth phenotype in case of IMS-PMD. "*+"indicates spots with further aggravation of growth phenotype due to deletion of TOM components. Porin (por1) deletion was taken as control. Time mentioned in hours at the upper right corner of the panel indicates the time of incubation of the spotted plates at 30°C before taking pictures. **C-D**. Drop-dilution assay as of MM-PMD (panel C) and IMS-PMD (panel D) strains with vms1Δ in presence and absence of the inducer. Vms1-HA expressed under endogenous promoter from a centromeric Ura plasmid has been shown to complement the growth defect observed in MM-PMD-vms1Δ. **+ indicates spots of MM-PMD-vms1Δ with further aggravation of growth phenotype of MM-PMD strain due to deletion of vms1. **E**. Western blot of Vms1-GFP protein expressed in MM-PMD-vms1Δ cells. Subcellular fractionation was done as described in methods section and equal amount of total protein from the whole cell lysate (WCL), mitochondrial fraction (Mito) and cytosolic fractions (cyto) were loaded and probed with anti-GFP antibody to detect the GFp-tagged Vms1 protein. Western blot from same fractions were also probed with Hsp60 and porin specific antibodies. **F**. Drop-dilution assay as of MM-PMD containing deletions of vms1 and other components of RQC and Vms1 interactors (rqc2, ltn1, doa1) in presence of the inducer. **+ indicates spots of MM-PMD-vms1Δ with further aggravation of growth phenotype of MM-PMD strain due to deletion of vms1 and "**-"indicates spots with alleviation of phenotype of MM-PMD due to deletion of rqc2, ltn1, rqc1 and doa1. **G.** Schematic picture showing domain organization of full length yeast Vms1 protein and its truncations mutants used in panel D. **H**. Drop-dilution assay as of MM-PMD-vms1Δ strain complemented with full length Vms1 and its truncation mutants expressed from centromeric Ura plasmid (as shown schematically in panel G) in presence and absence of the inducer. **+ indicates spots of MM-PMD-vms1Δ with further aggravation of growth phenotype of MM-PMD strain due to expression of non-functional Vms1ΔN mutant. All other strains containing Vms1 full

length or other truncation mutants can rescue the phenotype MM-PMD- vms1Δ and all are indicated by "**" signs.

Figure 7: A comprehensive model of IMS-UPR and mito-matrix-UPR

Upper panel (grey box): Step 1: Misfolded or aggregated protein from various sources, e.g. cytosolic protein which needs to be cleared by MAGIC, or mis-targeted proteins of neighbouring organelles like ER and cytosol or endogenous mutated or misfolded proteins accumulate in mitochondrial IMS and stress is mounted. **Step 2:** Stress leads to change in mitochondrial dynamics (severe fragmentation) and as a response TOM complex components are overexpressed. **Step 3:** TOM complex components possibly recruit proteases like Msp1, Ubx2 and helps in unclogging of blocked TOM translocase and may retrieve the misfolded/aggregated proteins from IMS followed by digestion of the misfolded/aggregated species. Due to long standing mitochondrial stress and decreased ATP production due to ineffective mitochondrial respiration, the translocation rate is decreased leading to cytosolic accumulation of mitochondrial precursor proteins. This in turn upregulates the cytosolic quality control machineries (cytoQC). **Step 4:** Successful step 3 leads to removal of stressor proteins and restoration of mitochondrial dynamics, function and cellular homeostasis. Step 3 is shown in red as we hypothesize the recruitment of proteases to TOM complex.

Lower panel (pink box): Step 1: Misfolded or aggregated protein from various sources, e.g. cytosolic protein which needs to be cleared by MAGIC, or mis-targeted proteins of neighbouring organelles like ER and cytosol or endogenous mutated or misfolded proteins accumulate in mitochondrial matrix and stress is mounted. **Step 2:** Stress leads to alteration in mitochondrial dynamics (severe fragmentation) and suspension of mitochondrial respiration as an adaptive response. **Step 3:** As a result of abrogated mitochondrial respiration, there is less ATP production leading to inefficient import of mitochondrial proteins, especially to matrix, which is an energy-dependent process. Reduced rate of translocation leads to stalling of translation associated translocation to mitochondria. **Step 4:** The stalled ribosome-nascent chain complex on mitochondria recruit the RQC complex and the nascent chains of mitochondrial precursors are CAT-tailed by Rqc2 with the help of Ltn1 and Rqc1. Antagonistic effect of Vms1 on Rqc2's CAT-tailing activity maintain a balance of amount of CAT-tailed precursors that ends up in mitochondria. **Step 5:** Inefficient or reduced translocation rate leads to accumulation of precursor proteins in cytosol (with and without CAT-tail) which ultimately mounts a stress in cytosol upregulating the cytosolic quality

control machineries (cytoQC). **Step 6:** In presence of Vms1, the balanced CAT-tailing of mitochondrial precursors by Rqc2 and Vms1 keep a check on the amount of CAT-tailed mitochondrial proteins. This along with cytoQC mediated clearing of accumulated precurosor in the cytoplasm brings back the cellular homeostasis. **Step 7 and 8:** In absence of functional Vms1, uncontrolled CAT-tailing by Rqc2 leads to accumulation of CAT-tailed proteins inside mitochondria which subsequently may aggregate and can exert additional proteotoxic stress in already stressed mitochondria. Step 8 is shown in red as we hypothesize the accumulation of CAT-tailed proteins in mitochondrial matrix. Additionally, Vms1's role in controlling the mitochondrial respiration during stress is absent which further pose problem leading to more stress and cell death in case of continued stress.

Material and Methods

Supplementary Table 1 contains the List of yeast strains, plasmids, primers and Antibodies and other reagents used for this study

Strains used: *S. cerevisiae* strain YMJ003 (*MATαhis3Δ1 leu2Δ0 met15Δ0 ura3Δ0 LYS+Δcan1::STE2*pr-*spHIS5 Δlyp1::STE3*pr-*LEU2 cyh2 Δura3*::UPRE-GFP-*TEF2*pr-RFP-*MET15-URA3*. BY4741 (*MATa, his3Δ1*; *leu2Δ0*; *met15Δ0*; *ura3Δ0*) [24] and *E.coli-DH5α* strains were used for this study. All the transformations and plasmid preparations were performed by standard method, which was adopted from the previous studies. Homologous recombination method was adapted for the generation of different compartment specific misfolding induced strains (Supplementary Table 1).

Construction of plasmids for homologous recombination to generate compartment specific misfolded protein strains in yeast

The construct of different compartment specific misfolded protein, the desired gene is amplified and cloned in *ApaI* and *AvrII* site of pYMN23 plasmid (Supplementary Table 1). The mitochondrial targeting signal sequence of yeast Cytochromeb2 (cyb2) was amplified from Cyb2-DHFR plasmid and was cloned upstream of the ORF to target the protein into mitochondrial inter-membrane space and the deletion of 19 amino acid membrane sorting signal (Cyb2Δ19) was done by overlap PCR from the Cyb2 sequence to target the proteins to

mitochondrial matrix. The whole construct is under the control of galactose inducible promoter. The whole DNA cassette was amplified by using Kapa HiFi DNA polymerase and transformed in yeast yMJ003 strain. Further, the integration of the DNA cassette at correct locus was confirmed by genotyping (plating on URA -/+ plates) and PCR based methods (using upstream and internal primers). Using similar methos, different constructs were prepared for different misfolded proteins which targets into different compartments (Supplementary Table 1). pVT100U-mtGFP plasmid was used as a fluorescent marker for mitochondria. For the localization study, misfolded protein (PMD) is tagged with GFP and integrated in the background strain as above.

Growth conditions and drop dilution assay

All the yeast strains are maintained at 30°C in the commercially available YEPD (1% Yeast extract, 2% Peptone and 2% Dextrose) medium in the presence of nourseothricin antibiotic (cloNAT) antibiotic selection. All the strains are grown in poorly-fementative YPR (1% Yeast extract, 2% Peptone and 2% Raffinose) medium overnight and re-inoculated in the same medium with the initial OD_{600} of 0.1. For drop dilution assay, the different strains were grown in YPR medium till 0.4-0.6 and serially diluted and spotted on different plates containing YP along with 2% dextrose (YPD) or 2% raffinose with (YPR+ gal) and without (YPR) 1%galactose or 3%glycerol (YPG), or for specific treatment with 10mM ascorbate, 10mM N-Acetyl Cysteine (NAC).

Crossing of misfolded protein expressing yeast strains with deletion strains from YKO library

Yeast strains carrying misfolded protein (referred nomenclature as mentioned in Supplementary Table 1) and genotype (*MATα his3Δ1 leu2Δ0 met15Δ0 ura3Δ0 LYS+Δcan1::STE2*pr-*spHIS5 Δlyp1::STE3*pr-*LEU2 cyh2 Δura3*::UPRE-GFP-*TEF2*pr-RFP-*MET15-URA3*::signal sequence misfolded protein-NAT derived from S288C), referred to as query strain here onwards, were crossed with knockout strain in BY4741 background (*MATa*, *his3Δ1*; *leu2Δ0*; *met15Δ0*; *ura3Δ0*;gene::KANMX) (Yeast KO Library, Mat A complete set, Thermofisher Scientific cat no. 95401.H2) as described previously [42]. Briefly, query strain and single KO strain were cultured in YPD media till saturation. 5ul from saturated culture of each strain were inoculated together into 400 µl of YPD in 2.2 ml 96 well deep-well plates and were co-cultured overnight for mating at 30°C, at 200 rpm continuous

shaking in a shaker incubator. For Mat a/ Mat α diploid selection, 10 µl of mated culture were re-inoculated in in 2.2 ml 96 well deep-well plates containing 400 µl of diploid selection medium (SD media with glutamic acid and without lysine, arginine and leucine) with antibiotics Nourseothricin 100 µg/ml and Geneticin 200µg/ml. The culture plate was incubated for 48 hours at 200 rpm continuous shaking at 30°. For sporulation, 10 µl of diploid cells were re-inoculated in 400 µl of sporulation medium (1% Potassium acetate, 0.1% Yeast extract, 0.05% Glucose, 0.1% Amino acid supplement powder from mixture containing 2 g histidine, 10 g leucine, 2 g lysine, and 2 g uracil) in 2.2 ml 96 well deep-well plates and the plates were incubated at 25° in static condition for 5 days. From sporulation media, 10 µl of culture was seeded in haploid selection media (SD without leu/Arg/Lys) along with canavanine and thialysine to select meiotic cells in Mat α background and plates were incubated at 30°C for next 2 days. Second round of haploid selection was done in similar manner in presence of antibiotics Nourseothricin and Geneticin. After the second round of haploid selection, strains were inoculated for genomic DNA isolation and were confirmed for KANMX cassette integration, gene deletion and mating type PCR.

Confocal microscopy imaging of yeast cells

Yeast cells were grown in YP-raffinose till it reaches the OD of 0.5 and the misfolded proteins were induced with addition of 1%galactose and further grown at 30C for 6-8hrs. Cells were harvested and washed once with 1XPBS. Cells were fixed with 3.5% formaldehyde solution and coated on Concanavalin A slides and allow 15mins for the cells to adhere on the slide and examined under confocal microscope. Images were captured in different positions of a slide and Z-series was acquired in each position. For the live-cell imaging, cells were coated on thin agarose gel pads and examined under microscope for different time-points.

Imaging of yeast mitochondria

Cells were transformed with pVT-100U-mtGFP and selected on SD-Ura plates. For microscopy, cells were grown in synthetic raffinose broth (SR-Ura medium) till the OD_{600} of 0.5. Cells were then induced with 1% galactose and were further grown at 30°C for 8-12hrs and then washed with 1X PBS and coated on concanavalin A slides. Imaging was done in Leica TCS SP8 confocal microscope.

Purification of mitochondria from yeast cells

Purification of yeast mitochondria was performed using standard protocol. Briefly, cells were grown in YP-raffinose medium till the $OD6_{00}$ of 0.4-0.6 and the strains were induced with 1% galactose and incubated at 30°C for 8hrs. Cells were harvested at 4,400xg and washed once and checked the wet weight of the cells. Then cells were suspended in 0.5g/ml of DTT buffer [100mM Tris/H_2SO_4 (pH 9.4), 10mM DTT] and incubated at 30°C for 30mins. Cells were spun down at 4,400xg and suspended in zymolyase buffer [20mM potassium phosphate (pH 7.4), 1.2 M sorbitol along with 2.5mg/gm Zymolyase 100T] and incubated at 30°C for 1hr. Cell wall digestion was checked in spectrophotometer. Further cells were pellet down at 3000xg at 4°C and re-suspended in 0.5mg/ml homogenization buffer [10mM Tris/HCl (pH 7.4), 0.6 M sorbitol, 1 mM EDTA, 0.2% (w/v) BSA] and homogenized 15 times by using Dounce homogenizer. The ruptured cell debris were collected by spin at 3000xg for 5mins at 4°C. The collected supernatant was spun down in high-speed at 12,000xg for 15mins at 4°C. The sedimented crude mitochondria was suspended in homogenization buffer. The slow speed and subsequent high speed centrifugation steps were repeated as described above. The resultant pellet contains crude mitochondria. Further the purified mitochondria was prepared by sucrose-gradient ultra-centrifugation. The different percentage of sucrose gradient was prepared in EM buffer [10mM MOPS/KOH (pH 7.2), 1mM EDTA]. First, 1.5ml of 60% sucrose in Beckman ultra-clear centrifuge tube was taken. Next, it was overlaid with 4ml of 32%, 1.5ml of 23% and 1.5ml of 15% sucrose to get the different gradients. The crude mitochondria was placed on top of 15% sucrose and centrifuge in Beckman SW41Ti swinging bucket rotor for 1hr at 1,34,000xg (33,000rpm) for 1hr at 4°C. The brown colored intact mitochondrial band was observed in between 60% and 32% sucrose interface. Mitochondrial band was carefully removed with cut micropipette tips and was placed it in Beckman centrifuge tube. The tube is filled with SEM buffer (10 mM MOPS/KOH pH 7.2, 250 mM Sucrose, 1 mM EDTA) and spin at 10,000xg for 30mins at 4°C. The resulting purified mitochondrial pellet was suspended in SH buffer (0.6M Sorbitol, 20mM HEPES pH 7.4) at the final concentration of 10mg/ml. Purified mitochondrial aliquots are made and are flash-frozen in liquid nitrogen and stored at -80°C for further use.

Measurement of oxygen consumption rate (OCR)

Yeast strains were grown in YPR and the secondary culture was induced at OD_{600} of 0.4-0.6 with 1% galactose and induced for 12 hours at 30°C. OD_{600} are checked after the induction and and cells are diluted with media (to OD_{600} of 1.0) and were used for checking the oxygen

consumption rate using Oxygraph (Oroboros) instrument. Initially the chambers were loaded with media to get the standard amount of oxygen present in the chamber, then the cells were loaded to measure the oxygen consumption. The uninduced cultures used as a control to measure the difference in oxygen consumption rate of the induced (stressed) cells due to proteotoxic stress.

Cloning of mitochondrial IMS or matrix targeted PMD for mammalian cell expression

Cloning of OCT-PMD (for specific targeting to mitochondrial matrix) and SMAC-PMD (for specific targeting to mitochondrial IMS) in pEGFP-N1 vector was achieved after amplification of the mitochondrial targeting sequence (MTS, OCT and SMAC) [43] and PMD by overlap PCR. In the first step, amplification of mitochondrial targeting signals and PMD gene sequence were done separately using gene specific set of primers with overhangs for overlap PCR. In the next step touchdown reaction was performed to overlap the PCR amplified products of MTS and PMD. In the final extension step, overlapped fragments were amplified to with the use of end primers (forward primer of MTS and reverse primer of PMD). OCT-PMD or SMAC-PMD sequences were cloned in pEGFPN1 vector in between XhoI and HindIII sites in frame with EGFP.

Confocal Imaging of mammalian cell (HeLa cells)

Confocal microscopy was performed using Nikon A1R MP+ Ti-E microscope system equipped with solid state lasers. All imaging was performed using Apochromat 100X 1.4 NA objective lens using oil immersion. 488nm and 561nm lasers were used to excite GFP and MitoTracker Red respectively, while 640nm lasers was used to excite far red signals. Prior to imaging cells were transfected with desired construct and incubated in CO_2 incubator for 16-20 hours.

Mitochondria Branch Length Measurement

Mitochondrial morphology and branch length were analyzed using Image J plugin MiNA (Mitochondrial Network Analysis) from (https://imagej.net/MiNA_-_Mitochondrial_Network_Analysis)[44]. Initially images were processed with Fiji software in the following order, granular noise were removed by following path; process →Noise→ Despeckle, to improve the image quality and mitochondrial visualization local contrast enhancement was performed by following path; Process→ Enhance Local Contrast (CLAHE). After pre-processing, Tubeness plugin of Imagej was used for mitochondrial

segmentation and clear visualization of mitochondrial network by following path Plugins→ Analyze→ Tubeness. Finally, MiNA plugin was used to calculate mitochondrial mean branch length by following path Plugins→ Stuart Lab→ MiNA Scripts→ MiNA Analyze Morphology. Statistical analysis by the Student's t-test.

Cell Cytotoxicity Assay

To perform cell cytotoxicity assay ~ 10,000 HeLa cells were seeded per well in 96 well plate and incubated in CO_2 incubator for 24 hours. After that transfection with OCT/SMAC-PMD-GFP and control DNA, plate was kept in the incubator for next 48 hours. After 48 hours incubation, cytotoxicity assay was performed using CyQUANT^{TM} LDH Cytotoxicity Assay kit (Invitrogen) following the manufacturer's protocol.

RNA isolation and RNA sequencing

Yeast cells were grown and induced with 1% galactose in YPR media for 4hrs, 8hrs, 12hrs or 16hrs and un-induced cells were kept as controls. After growth, cells were harvested at 6000 rpm for 15mins at 4°C. After centrifugation, the cell pellet was washed with chilled 1X PBS; re-suspended in 1 ml of sterile, chilled 1X PBS (pH 7.4) and was transferred to a sterile microfuge tube. Tubes were centrifuged at 12,000 rpm for 5mins at 4°C and the supernatant was discarded carefully. Acid washed glass beads were added to the pellet (two times the volume of the pellet). To this, 1ml Trizol was added to each tube and kept on bead beater for a total of 5-6mins such that it was on the bead beater for 1 min and on ice for the next 2-3mins. Following this, it was spun down on a table-top centrifuge and the supernatant was collected in a fresh centrifuge tube. To the supernatant, chloroform was added (250µl chloroform was added to 800µl of the supernatant) and was vortexed till the solution turned milky pink. This was further incubated at room temperature for 10mins and then centrifuged at 13,000 rpm for 15mins at 4°C. The aqueous phase on top was collected very carefully without disturbing the white layer in the middle, in a fresh centrifuge tube. To this supernatant, 1mL of isopropanol was added, mixed by rotating and kept at -20°C for 2hours. This was then centrifuged at 13,000rpm for 30mins at 4°C. The supernatant was discarded and 750µl of chilled 80% ethanol was used to wash the pellet. The tubes were kept open for air drying the pellet and the pellet was finally re-suspended in 60µl of sterile, nuclease free water. The RNA was visually inspected on ethidium bromide-stained agarose gel to verify the integrity of RNA. Using TruSeq RNA sample prep kit v2 (Stranded mRNA LT kit), the transcriptomic library was prepared according to the manufacturer's instructions

(www.illumina.com). Briefly, 700ng of RNA with high purity and integrity from each sample was used to generate the library. Adaptor-ligated fragments were purified using AMPure XP beads (Agencourt). The library thus generated was run on BioAnalyzer DNA1000 LabChip (Agilent Technologies) to determine the fragment size. The concentration was estimated using Qubit high sensitivity (HS) kit for double stranded DNA on the Qubit instrument (Invitrogen). The average fragment size of the libraries was determined with a BioAnalyzer DNA1000 LabChip (Agilent Technologies). Diluted libraries were multiplex-sequenced and run on a HiSeq 2000 Illumina platform in HiSeq Flow Cell v3 (Illumina Inc., USA) using TruSeq SBS Kit v3 (Illumina Inc., USA) for cluster generation as per manufacturer's protocol. All transcriptomic were performed with two biological replicates of each sample. From the bcl files that were generated after sequencing, .fasta files were created. FastQ was used to check the quality of the reads. Reads with Phred score of 30 or above were taken forward for further analysis. Trimmomatic (v0.43) was used to trim the read sequences, if required. The resulting reads were then aligned to the transcriptome of *S. cerevisiae* strain S288c as available from ENSEMBL. Kallisto was used to perform the alignment and we had a minimum of 80% alignment to the reference. Using Kallisto, we were able to estimate gene expression levels as TPM (transcripts per million) values.

Transcriptome Data Analysis

The transcriptome data was analyzed with a standard Kallisto pipeline as described previously [45]. Briefly, fastq files were trimmed using Trimmomatic and the fastqc files were aligned to the yeast transcriptome using Kallisto. The TPM values that were obtained were used to analyze the fold changes. Two types of analysis were performed. First, we used a large-scale RNA-seq with 46 samples (uninduced and induced cells of Wt and misfolded protein expressing to specific sub-cellular compartments namely mitochondrial IMS, mitochondrial matrix, ER, cytosol and nucleus). With 39 samples we could verify that the expression patterns of each gene which were normally distributed about their mean over the different conditions. To check if a gene is significantly upregulated or downregulated in a particular sample, we obtained the Z-score value for each gene, with the mean and standard deviation obtained over all the conditions. For each condition, genes that had a Z-score > 2 or <-2 were used to obtain condition-specific upregulated or downregulated gene list, respectively. Second, for time course analysis of transcriptome we performed RNA-seq for the strains (IMS-DMMBP, IMS-PMD with IMS-MBP strain as control and MM-DMMBP, MM-PMD with MM-MBP strain as control) at 0hrs, 4 hrs, 8 hrs and 12 hrs post induction of

the exogenous proteins. The TPM values were quantile normalized, averaged over replicates and fold change was calculated with respect to 0hrs TPM value (un-induced set) for each of the compartment-specific targeted exogenous proteins. The fold change values were then used to obtain gene-set specific information using R-package.

Mass Spectrometry

Yeast strains (Wt, IMS-PMD and MM-PMD) were grown overnight in YPR. Next morning, secondary culture was inoculated at OD_{600} of 0.1 and grown till OD_{600} of 0.5. Each culture was divided in two culture tubes and in one half of each strain was induced with 1% galactose for 12 hours. The other half was grown in YPR as uninduced controls. After induction, equal number of cells were taken from uninduced and induced culture of each strain, cells were harvested by centrifugation and were re-suspended in resuspension buffer (50mM Tris-HCl, pH 7.5, 150 mM NaCl, 1mM EDTA, 5mM $MgCl_2$, 1% NP-40, Protease inhibitor cocktail). The re-suspended cells were subjected to lysis by using glass beads in bead beater. Each cycle of bead beating of 3 minutes were followed by incubation in ice for 5 minutes and 3-4 cycles of bead beating were done. After cell lysis, the whole cell lysate were centrifuged at 18,000Xg for 15 minutes and the supernatant were collected in fresh tubes. All lysates were quantified by BCA protein estimation kit (Thermo Scientific) and the concentrations were made equal for all samples (~10mg/ml). The whole cell lysates were boiled at 95°C for 10 minutes with 4X SDS loading buffer [0.2 M Tris–HCl (pH 6.8), 8% SDS, 0.05 M EDTA, 4% 2-mercaptoethanol, 40% glycerol, 0.8% bromophenol blue] and heating at 95□ for 10 min and were centrifuged shortly to remove the debris. 150 µg of protein extract from each sample were ran on NuPAGE 4%–12% Bis–Tris Protein Gels (Invitrogen) using MES running buffer (100 mM MES, 100 mM Tris–HCl, 2 mM EDTA, 7 mM SDS) at 200 V for 40 min and fixed and stained with Coomassie brilliant blue. Reduction, alkylation and In-gel trypsin digestion was done as described in Shevchenko et al [46]. Trypsin digested peptides were eluted, desalted and vacuum dried as described in Rappsilber et al [47], and stored in -20□ until Mass spectrometry analysis.

Dried peptides were dissolved in 2% formic acid and sonicated in bath sonication for 5 min. Each sample were loaded in reverse phase liquid chromatography followed by mass spectrometry analysis. Peptides were analysed on Q Exactive (Thermo Scientific) mass spectrometer interfaced with nano- flow LC system (Easy nLC II, Thermo Scientific). EasySpray Nano Column PepMap™ RSLC C18 (Thermo Fisher) (75 µm× 15 cm; 3 µm;

100Å) using 60 min gradient of mobile phase [5% Can containing 0.1% formic acid (buffer A) and 90% ACN (acetonitrile) containing 0.1% formic acid (buffer B)] at flow rate 300nL/min was used for separation of peptide. Full scan of MS spectra (from/z 400 to 1650) were acquired followed by MS/MS scans of top 10peptide with charge state 2 of higher.

Raw files obtained were analysed in MaxQuant Computational platform (Ver. 1.6.10.43) using UniProt database of *Saccharomyces cerevisiae* (released Nov, 2019) [48]. LFQ option was selected for label free quantification with minimum 2 unique peptides for ratio count along with oxidation (M), acetylation (Protein N-term) as variable and carbomethylation as fixed modification. Additional parameters: 2 trypsin missed cleavages, 20 ppm peptide mass tolerance and 1% peptide false discovery rate (FDR) were allowed. Further data analysis and statistical tests were performed in Perseus (Ver. 1.6.0.2) [49].

To compare the control and stressed samples, ratio of IMS-PMD by control and MM-PMD by control is calculated using average LFQ intensities of two biological repeat experiments. The ratio is converted into Log2 space and mean and standard deviation is calculated for both conditions. Z-score normalization was done for both conditions using the formula

$$\text{z} - \text{score of [x]} = \frac{\log_2 \left(\frac{\text{PMD-IMS or PMD MM}}{\text{Control}}\right)[x] - \text{Mean of } \log_2 (a \ldots n)}{\text{Standard deviation of } \log_2 (\text{a} \ldots . \text{n})}$$

where X is single protein and “a” to “n” is dataset of proteins.

Z-score cut-off ±1.96 indicates population lies outside the 95 % interval hence considered significant. The z-score cut-off (1≤ Z) and (-1≥ Z) of proteins is considered as enriched and depleted respectively. Heatmaps were prepared using Morphius (https://software.broadinstitute.org/morpheus).

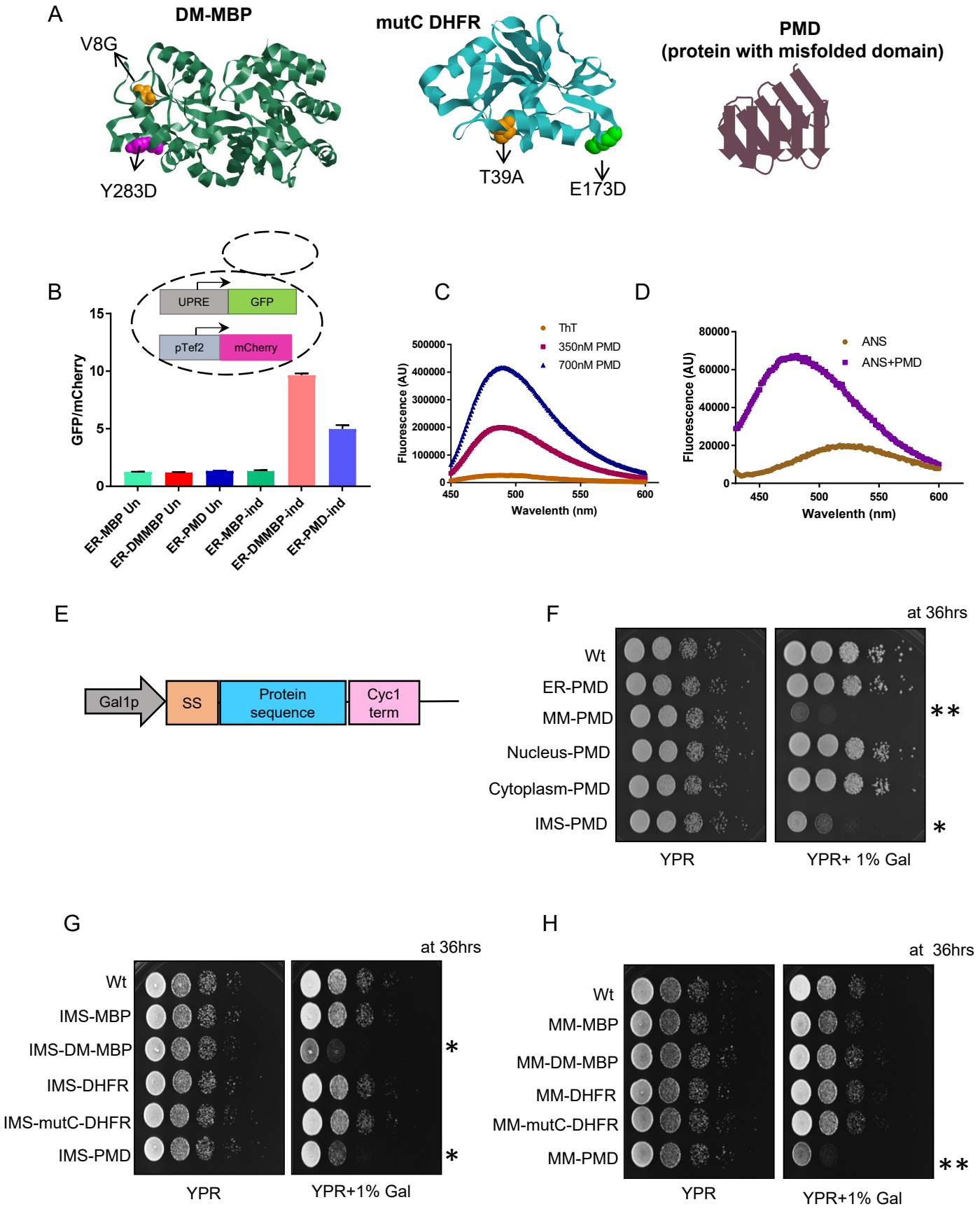
A
DM-MBP
V8G
Y283D
mutC DHFR
T39A
E173D
PMD
(protein with misfolded domain)
B
UPRE
GFP
pTef2
mCherry
GFP/mCherry
ER-MBP Un
ER-DMMBP Un
ER-PMD Un
ER-MBP-ind
ER-DMMBP-ind
ER-PMD-ind
C
ThT
350nM PMD
700nM PMD
Fluorescence (AU)
Wavelenth (nm)
D
ANS
ANS+PMD
Fluorescence (AU)
Wavelenth (nm)
E
Gal1p
SS
Protein sequence
Cyc1 term
F
at 36hrs
Wt
ER-PMD
MM-PMD
Nucleus-PMD
Cytoplasm-PMD
IMS-PMD
YPR
YPR+ 1% Gal
G
at 36hrs
Wt
IMS-MBP
IMS-DM-MBP
IMS-DHFR
IMS-mutC-DHFR
IMS-PMD
YPR
YPR+1% Gal
H
at 36hrs
Wt
MM-MBP
MM-DM-MBP
MM-DHFR
MM-mutC-DHFR
MM-PMD
YPR
YPR+1% Gal

Figure 1

A

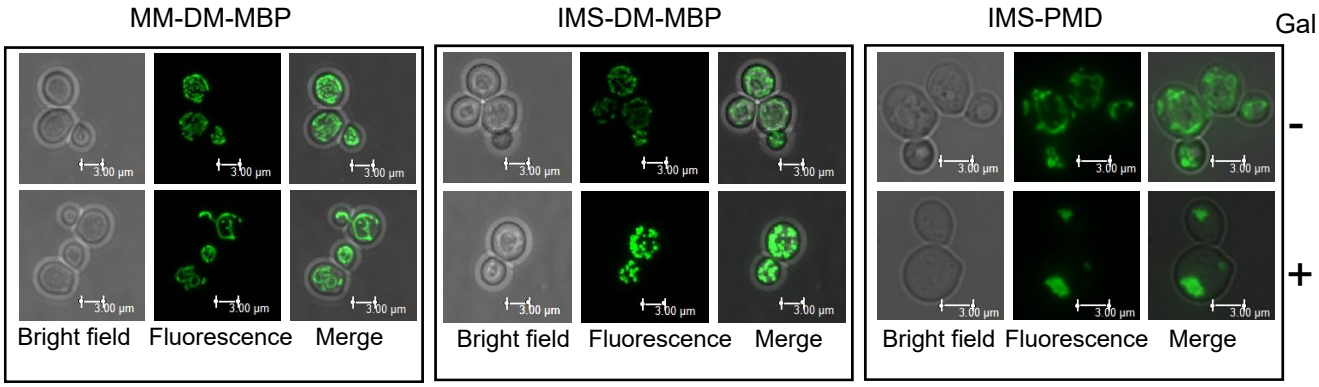
MM-DM-MBP
IMS-DM-MBP
IMS-PMD
Gal
-
+
Bright field
Fluorescence
Merge
Bright field
Fluorescence
Merge
Bright field
Fluorescence
Merge

B

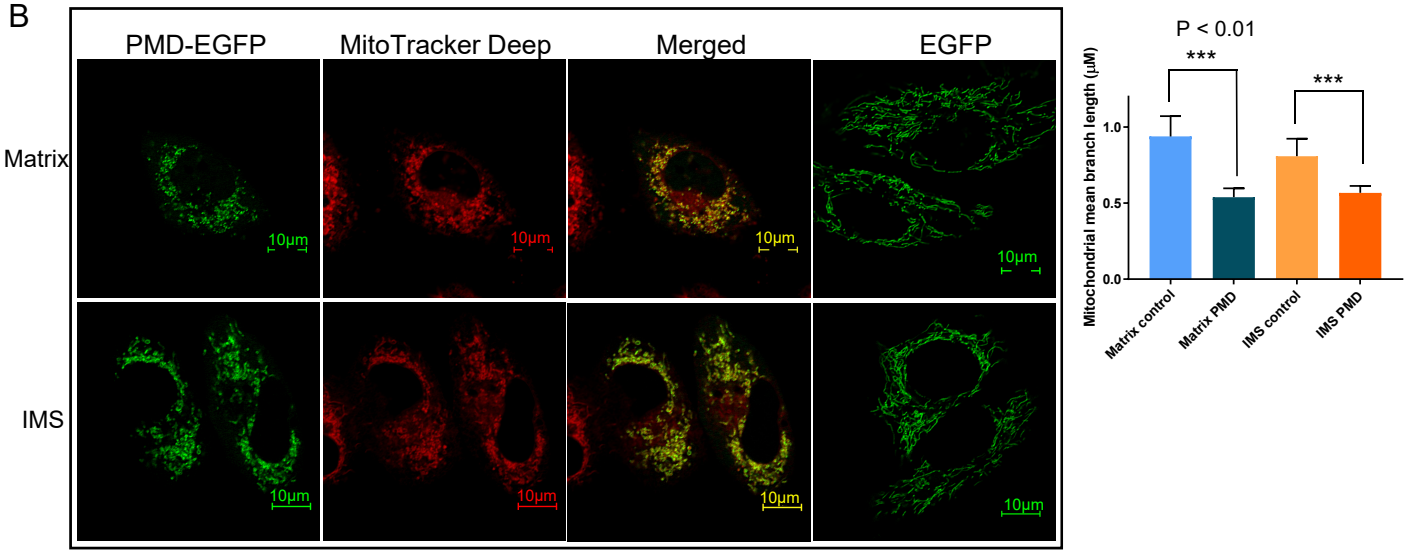
PMD-EGFP
MitoTracker Deep
Merged
EGFP
Matrix
IMS
10μm
P < 0.01
***
***
Mitochondrial mean branch length (μM)
1.0
0.5
0.0
Matrix control
Matrix PMD
IMS control
IMS PMD

C

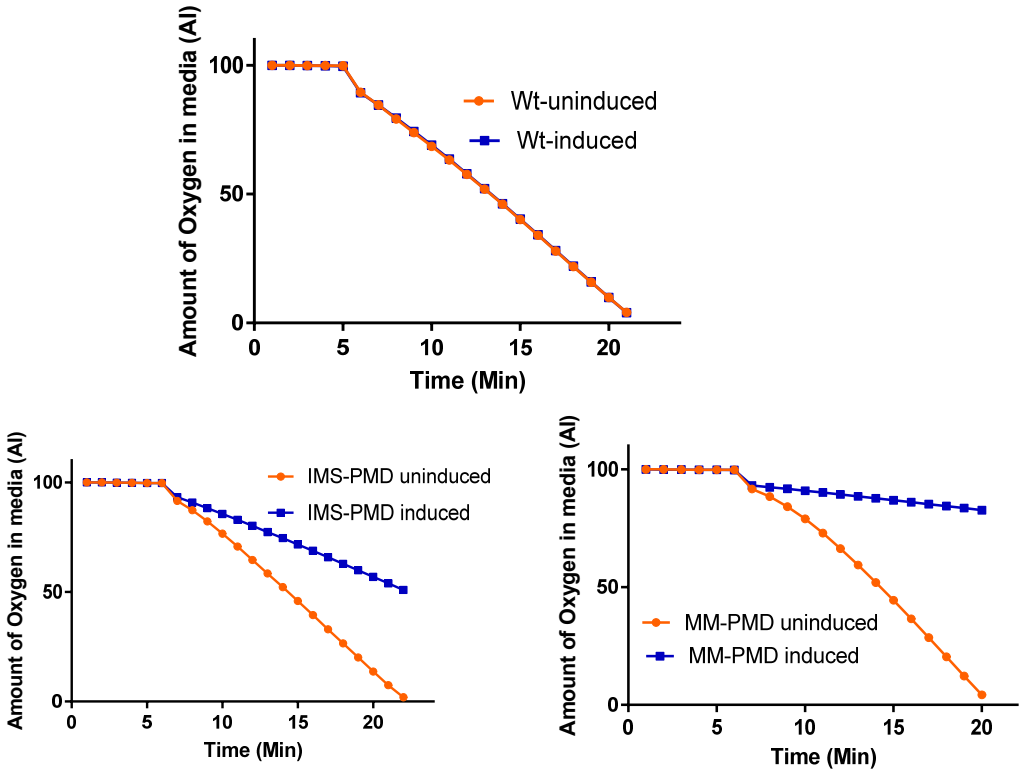
Amount of Oxygen in media (AI)
100
50
0
0
5
10
15
20
Time (Min)
Wt-uninduced
Wt-induced
IMS-PMD uninduced
IMS-PMD induced
MM-PMD uninduced
MM-PMD induced

Figure 2

A

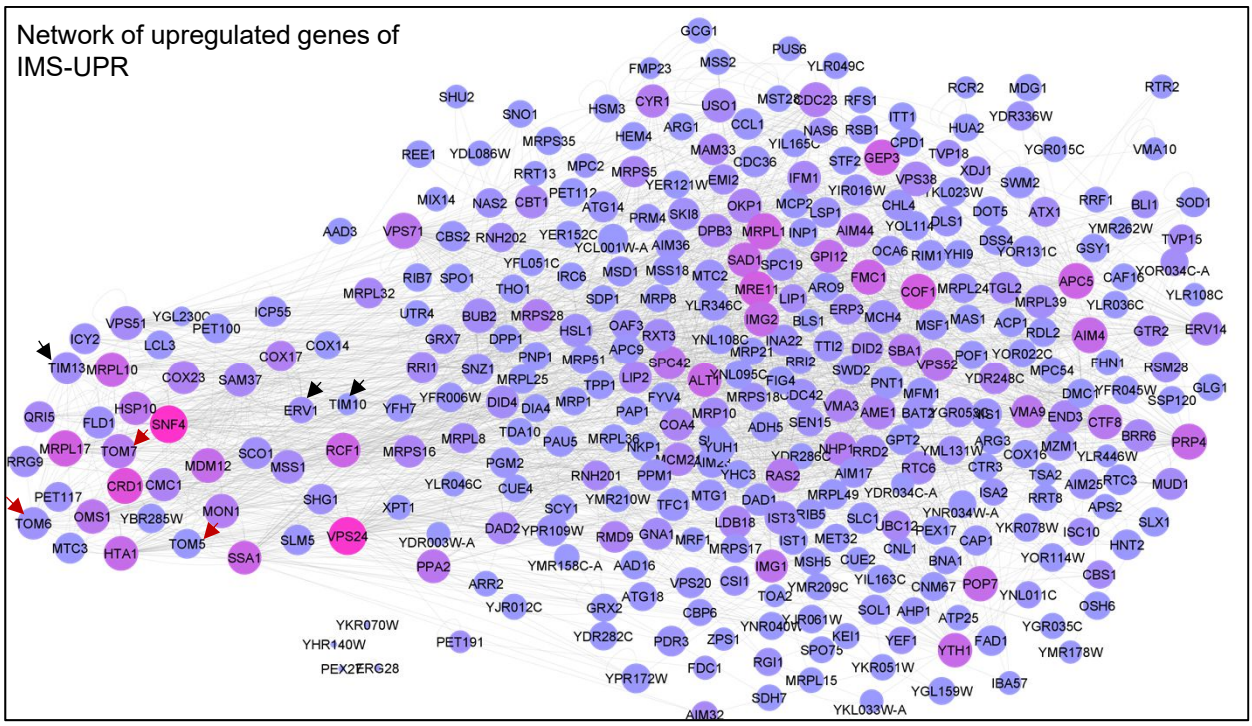
Network of upregulated genes of
IMS-UPR

B

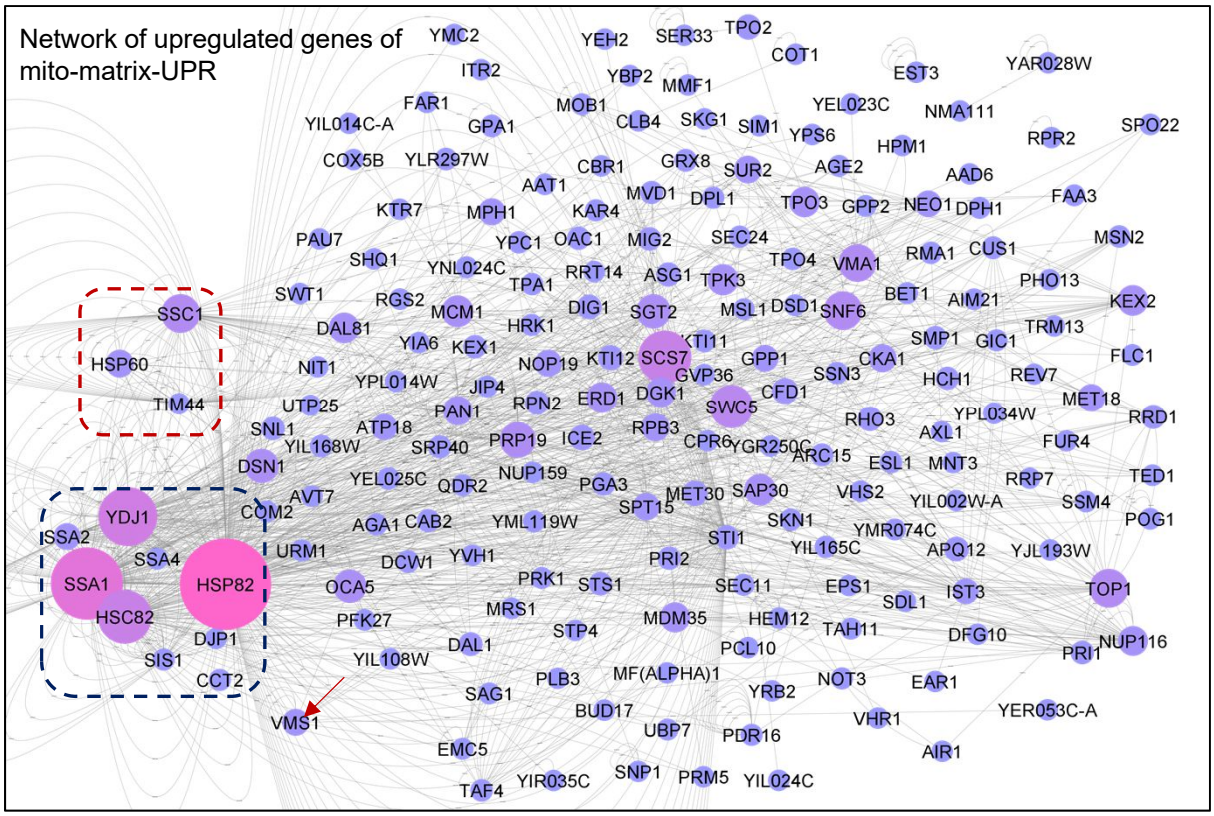
Network of upregulated genes of
mito-matrix-UPR
SSC1
HSP60
TIM44
YDJ1
SSA2
SSA4
SSA1
HSP82
HSC82
DJP1
SIS1
CCT2
VMS1

Figure 3

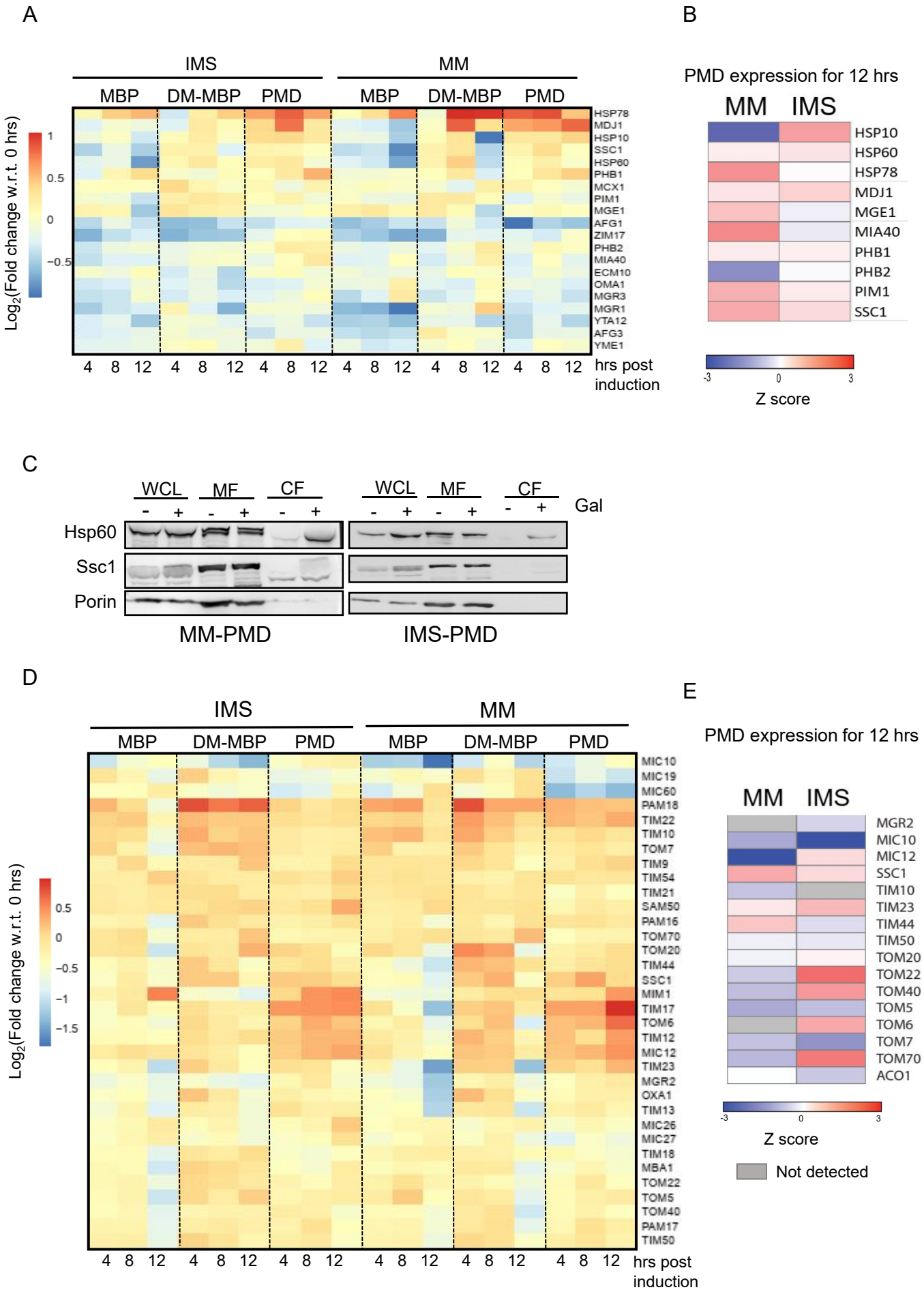
A
IMS
MM
MBP
DM-MBP
PMD
MBP
DM-MBP
PMD
Log2(Fold change w.r.t. 0 hrs)
1
0.5
0
−0.5
HSP78
MDJ1
HSP10
SSC1
HSP60
PHB1
MCX1
PIM1
MGE1
AFG1
ZIM17
PHB2
MIA40
ECM10
OMA1
MGR3
MGR1
YTA12
AFG3
YME1
4 8 12 4 8 12 4 8 12 4 8 12 4 8 12 4 8 12
hrs post induction
B
PMD expression for 12 hrs
MM IMS
HSP10
HSP60
HSP78
MDJ1
MGE1
MIA40
PHB1
PHB2
PIM1
SSC1
-3
0
3
Z score
C
WCL
MF
CF
WCL
MF
CF
- + - + - + - + - + - +
Gal
Hsp60
Ssc1
Porin
MM-PMD
IMS-PMD
D
IMS
MM
MBP
DM-MBP
PMD
MBP
DM-MBP
PMD
Log2(Fold change w.r.t. 0 hrs)
0.5
0
−0.5
−1
−1.5
MIC10
MIC19
MIC60
PAM18
TIM22
TIM10
TOM7
TIM9
TIM54
TIM21
SAM50
PAM16
TOM70
TOM20
TIM44
SSC1
MIM1
TIM17
TOM6
TIM12
MIC12
TIM23
MGR2
OXA1
TIM13
MIC26
MIC27
TIM18
MBA1
TOM22
TOM5
TOM40
PAM17
TIM50
4 8 12 4 8 12 4 8 12 4 8 12 4 8 12 4 8 12
hrs post induction
E
PMD expression for 12 hrs
MM IMS
MGR2
MIC10
MIC12
SSC1
TIM10
TIM23
TIM44
TIM50
TOM20
TOM22
TOM40
TOM5
TOM6
TOM7
TOM70
ACO1
-3
0
3
Z score
Not detected

Figure 4

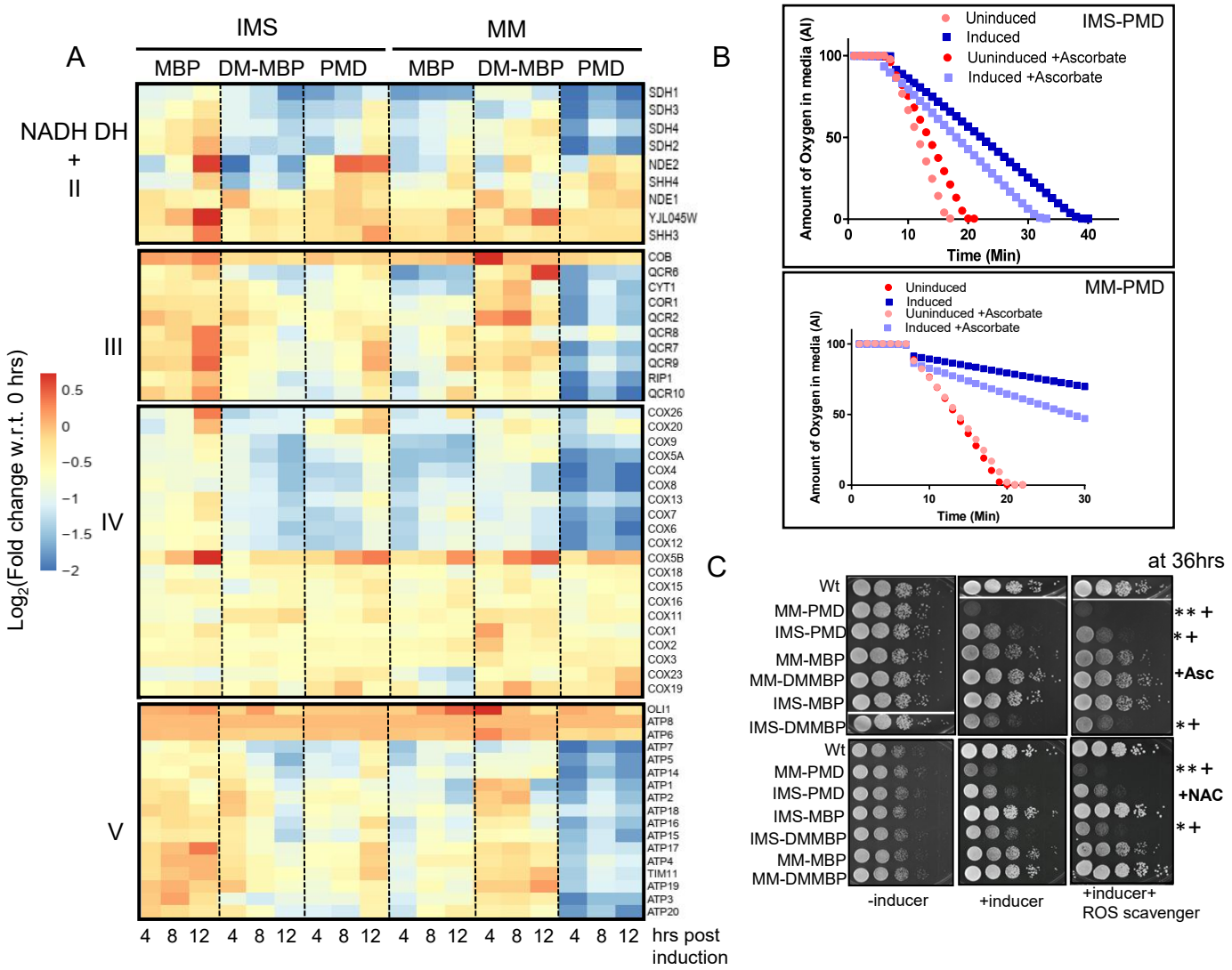
A
IMS
MM
MBP
DM-MBP
PMD
NADH DH + II
III
IV
V
Log2(Fold change w.r.t. 0 hrs)
0.5
0
−0.5
−1
−1.5
−2
SDH1
SDH3
SDH4
SDH2
NDE2
SHH4
NDE1
YJL045W
SHH3
COB
QCR6
CYT1
COR1
QCR2
QCR8
QCR7
QCR9
RIP1
QCR10
COX26
COX20
COX9
COX5A
COX4
COX8
COX13
COX7
COX6
COX12
COX5B
COX18
COX15
COX16
COX11
COX1
COX2
COX3
COX23
COX19
OLI1
ATP8
ATP6
ATP7
ATP5
ATP14
ATP1
ATP2
ATP18
ATP16
ATP15
ATP17
ATP4
TIM11
ATP19
ATP3
ATP20
4 8 12 4 8 12 4 8 12 4 8 12 4 8 12 4 8 12
hrs post induction
B
IMS-PMD
Uninduced
Induced
Uuninduced +Ascorbate
Induced +Ascorbate
Amount of Oxygen in media (AI)
Time (Min)
MM-PMD
C
at 36hrs
Wt
MM-PMD
IMS-PMD
MM-MBP
MM-DMMBP
IMS-MBP
IMS-DMMBP
+Asc
+NAC
-inducer
+inducer
+inducer+ ROS scavenger
D
Upregulated
Downregulated
T: transcriptomics
P: proteomics
Glucose
HXK1
Glucose 6-phosphate
PGI1
Fructose 6-phosphate
PFK1
Fructose 1-6-bisphosphate
FBA1
Glyceraldehyde 3-phosphate
TDH1
TDH2
TDH3
3-phospho D glyceroyl phosphate
PGK1
3-phosphoglycerate
GPM1
3-phosphoenolpyruvate
PYK1/CDC19
PYK2
Pyruvate
PYC1
PYC2
Oxaloacetate
MDH1
Malate
FUM1
Fumerate
SDH1
SDH2
SDH3
SDH4
Succinate
LSC1
LSC2
Succinyl CoA
LPD1
KGD1
KGD2
α-keto glutarate
IDH1
IDH2
Isocitrate
ACO1
Cis-aconitate
ACO2
Citrate
CIT1
CIT3

Figure 5

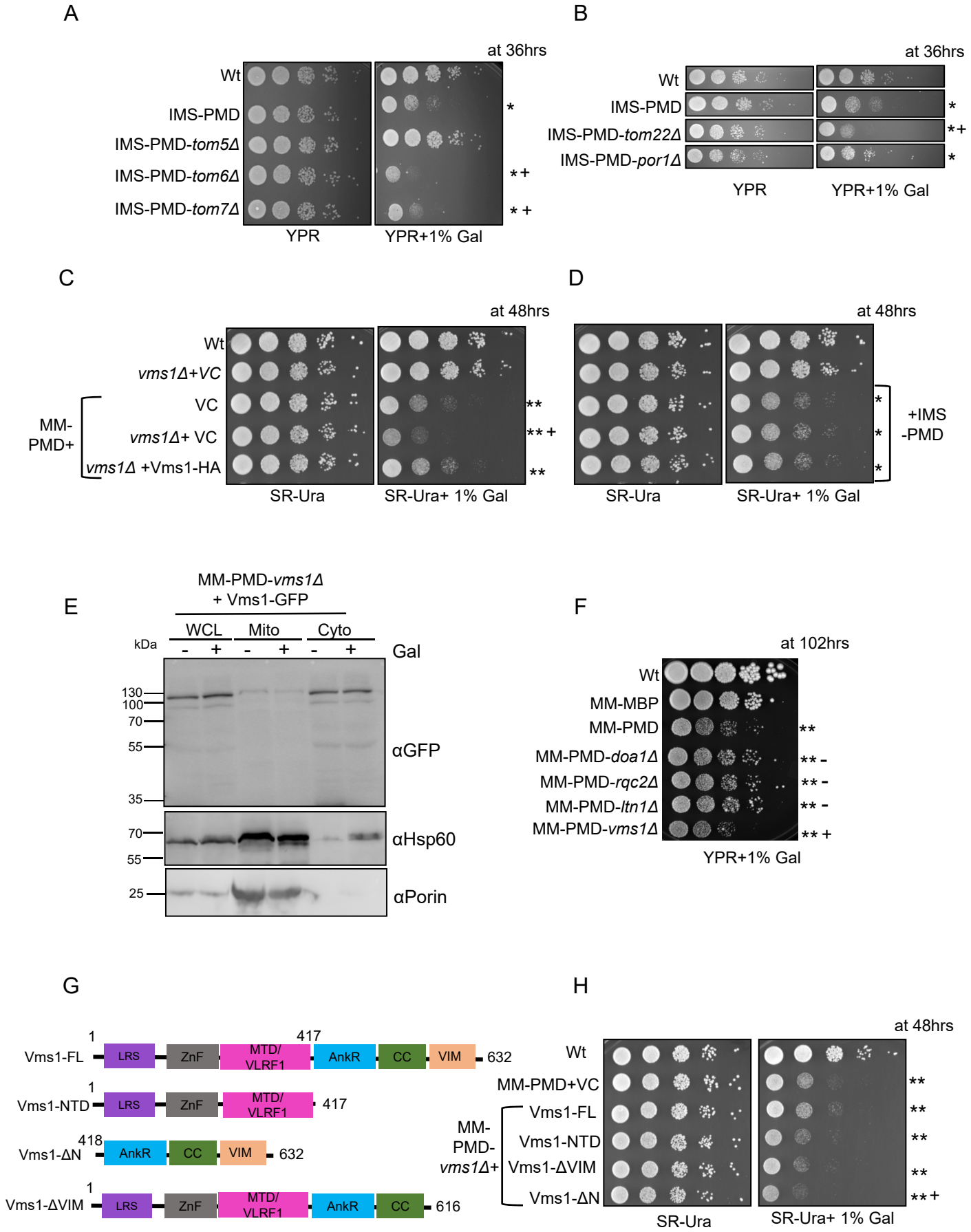
A
at 36hrs
Wt
IMS-PMD
IMS-PMD-tom5Δ
IMS-PMD-tom6Δ
IMS-PMD-tom7Δ
YPR
YPR+1% Gal
B
at 36hrs
Wt
IMS-PMD
IMS-PMD-tom22Δ
IMS-PMD-por1Δ
YPR
YPR+1% Gal
C
at 48hrs
Wt
vms1Δ+VC
VC
vms1Δ+ VC
vms1Δ +Vms1-HA
MM-PMD+
SR-Ura
SR-Ura+ 1% Gal
D
at 48hrs
+IMS -PMD
SR-Ura
SR-Ura+ 1% Gal
E
MM-PMD-vms1Δ + Vms1-GFP
WCL
Mito
Cyto
kDa
Gal
αGFP
αHsp60
αPorin
F
at 102hrs
Wt
MM-MBP
MM-PMD
MM-PMD-doa1Δ
MM-PMD-rqc2Δ
MM-PMD-ltn1Δ
MM-PMD-vms1Δ
YPR+1% Gal
G
Vms1-FL
Vms1-NTD
Vms1-ΔN
Vms1-ΔVIM
LRS
ZnF
MTD/ VLRF1
AnkR
CC
VIM
H
at 48hrs
Wt
MM-PMD+VC
MM-PMD-vms1Δ+
Vms1-FL
Vms1-NTD
Vms1-ΔVIM
Vms1-ΔN
SR-Ura
SR-Ura+ 1% Gal

Figure 6

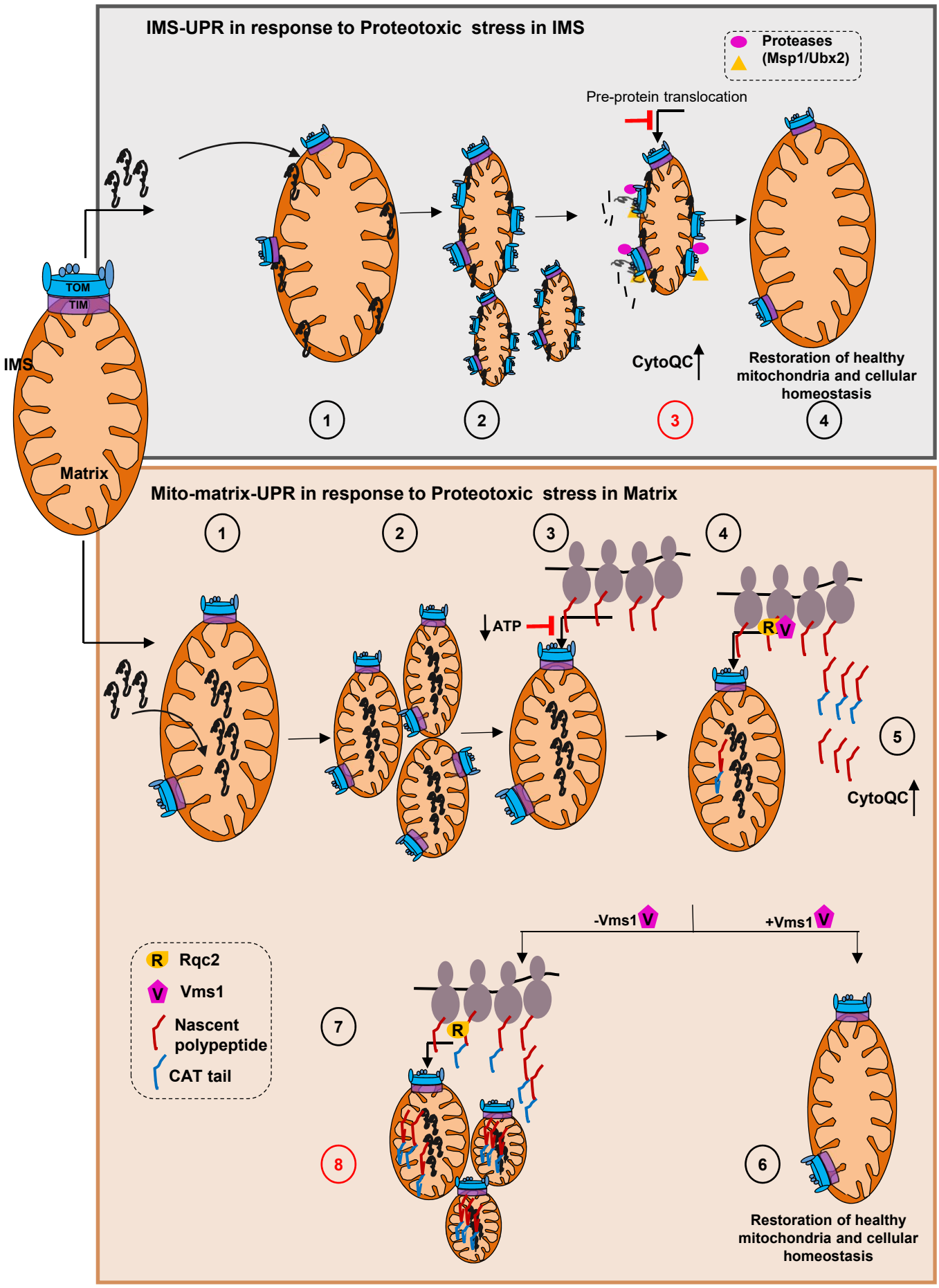
IMS-UPR in response to Proteotoxic stress in IMS
Proteases
(Msp1/Ubx2)
Pre-protein translocation
TOM
TIM
IMS
Matrix
CytoQC
Restoration of healthy mitochondria and cellular homeostasis
1
2
3
4
Mito-matrix-UPR in response to Proteotoxic stress in Matrix
ATP
R
V
5
CytoQC
-Vms1
+Vms1
Rqc2
Vms1
Nascent polypeptide
CAT tail
7
8
6
Restoration of healthy mitochondria and cellular homeostasis

Figure 7

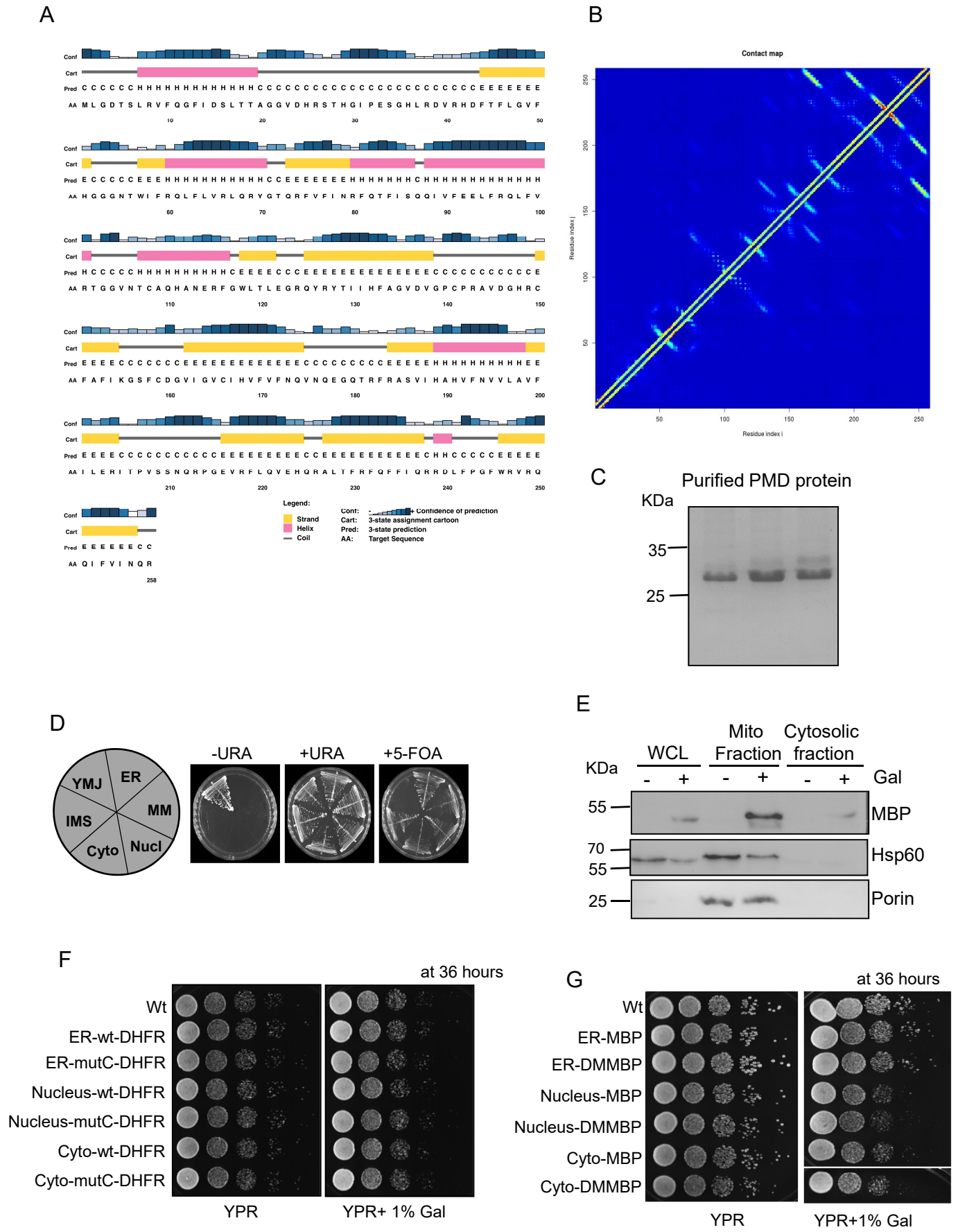
A
B
Contact map
Residue index i
C
Purified PMD protein
KDa
35
25
D
YMJ
ER
MM
IMS
Cyto
Nucl
-URA
+URA
+5-FOA
E
KDa
WCL
Mito Fraction
Cytosolic fraction
- + - + - +
Gal
55
MBP
70
55
Hsp60
25
Porin
F
at 36 hours
Wt
ER-wt-DHFR
ER-mutC-DHFR
Nucleus-wt-DHFR
Nucleus-mutC-DHFR
Cyto-wt-DHFR
Cyto-mutC-DHFR
YPR
YPR+ 1% Gal
G
at 36 hours
Wt
ER-MBP
ER-DMMBP
Nucleus-MBP
Nucleus-DMMBP
Cyto-MBP
Cyto-DMMBP
YPR
YPR+1% Gal

Figure S1

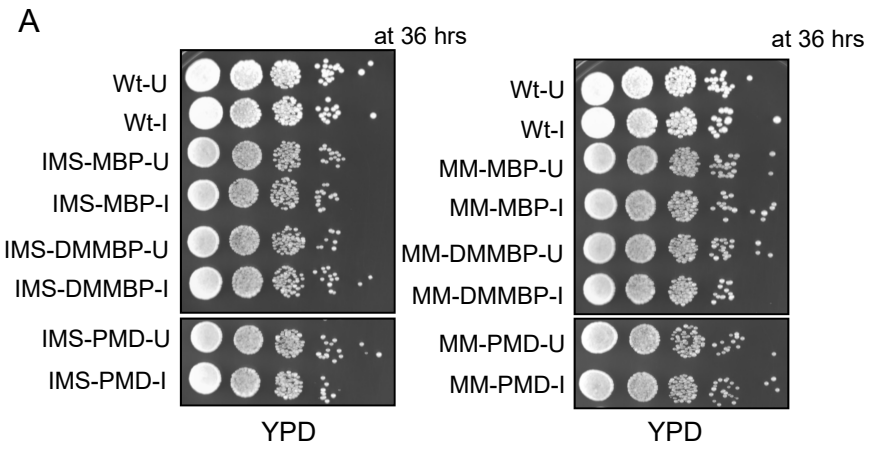
A
at 36 hrs
Wt-U
Wt-I
IMS-MBP-U
IMS-MBP-I
IMS-DMMBP-U
IMS-DMMBP-I
IMS-PMD-U
IMS-PMD-I
YPD
at 36 hrs
Wt-U
Wt-I
MM-MBP-U
MM-MBP-I
MM-DMMBP-U
MM-DMMBP-I
MM-PMD-U
MM-PMD-I
YPD

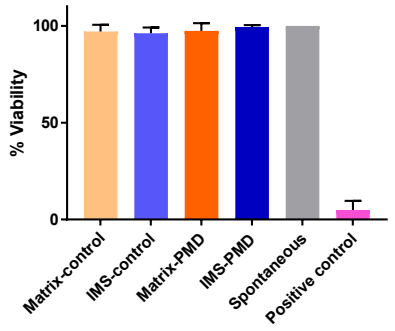
D
% Viability
100
50
0
Matrix-control
IMS-control
Matrix-PMD
IMS-PMD
Spontaneous
Positive control

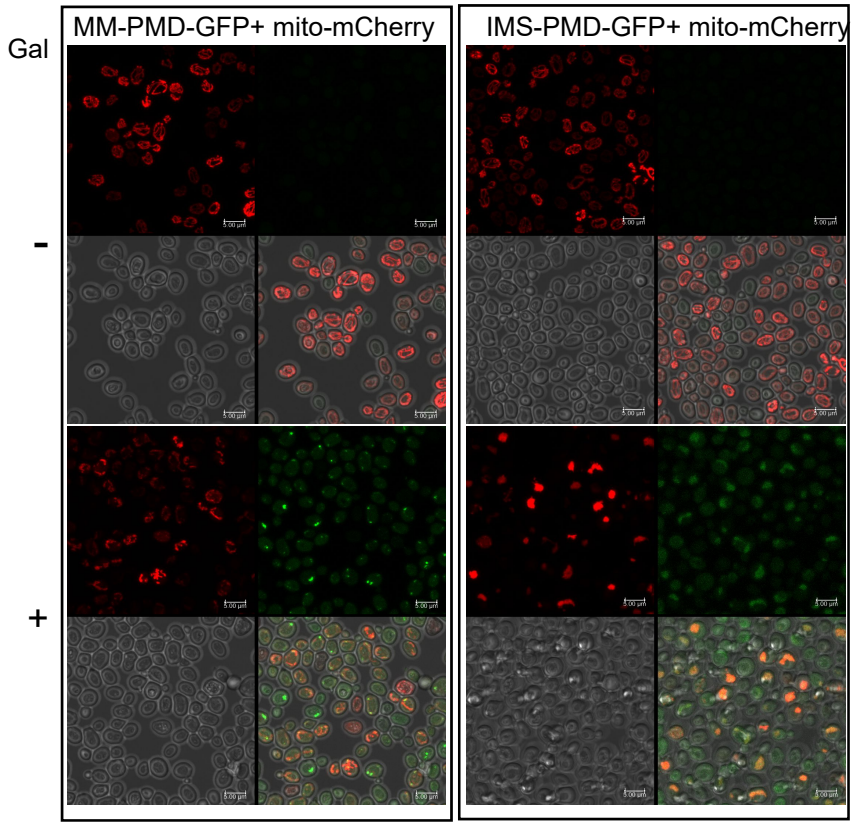
B
Gal
-
+
MM-PMD-GFP+ mito-mCherry
IMS-PMD-GFP+ mito-mCherry

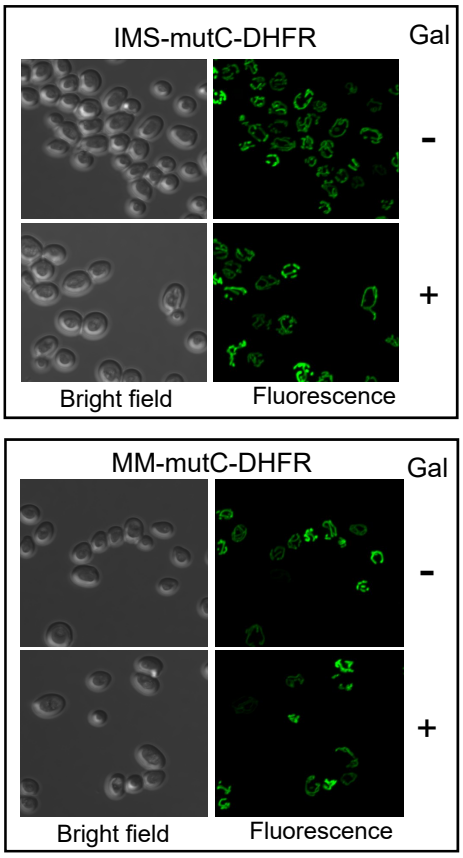
C
IMS-mutC-DHFR
Gal
-
+
Bright field
Fluorescence
MM-mutC-DHFR
Gal
-
+
Bright field
Fluorescence

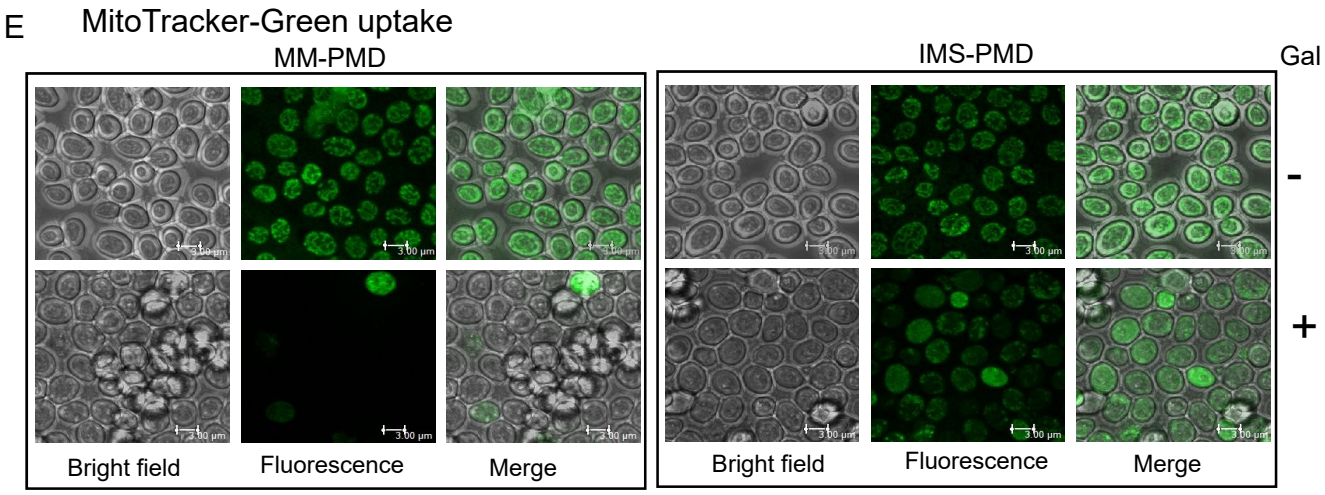
E
MitoTracker-Green uptake
MM-PMD
IMS-PMD
Gal
-
+
Bright field
Fluorescence
Merge
Bright field
Fluorescence
Merge

Figure S2

A Genetic interaction with mitochondrial chaperones during misfolding stress

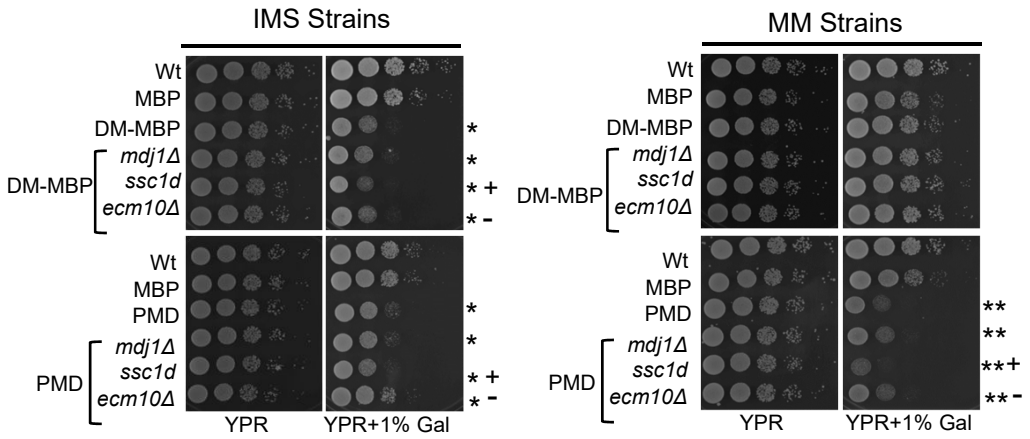

B Genetic interaction mitochondrial proteases during misfolding stress

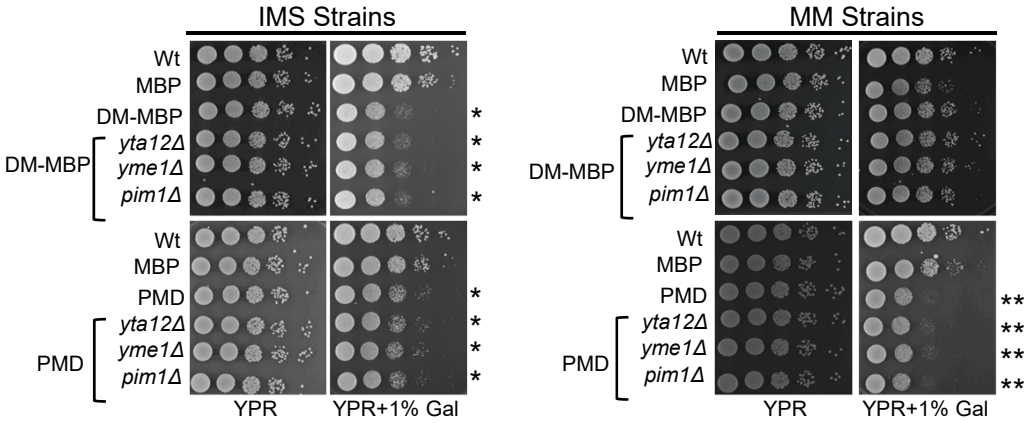

C Genetic interaction of with differentially upregulated genes during misfolding stress

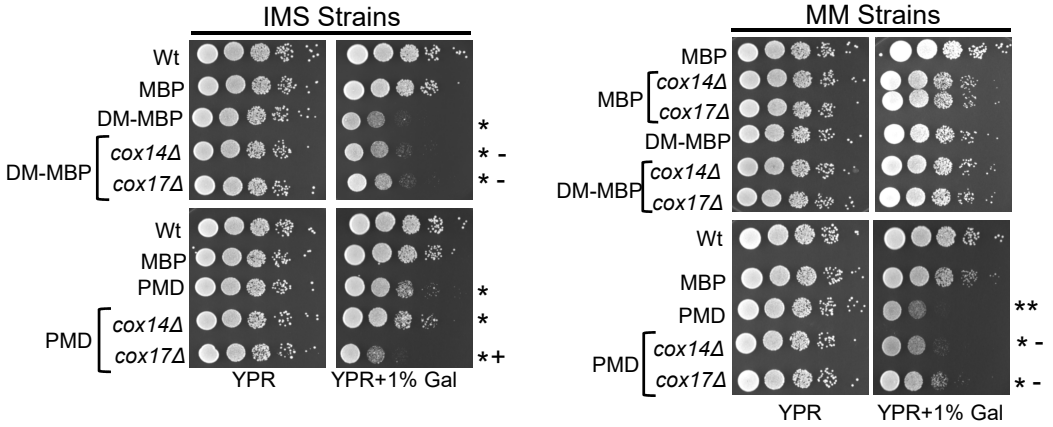

Figure S3

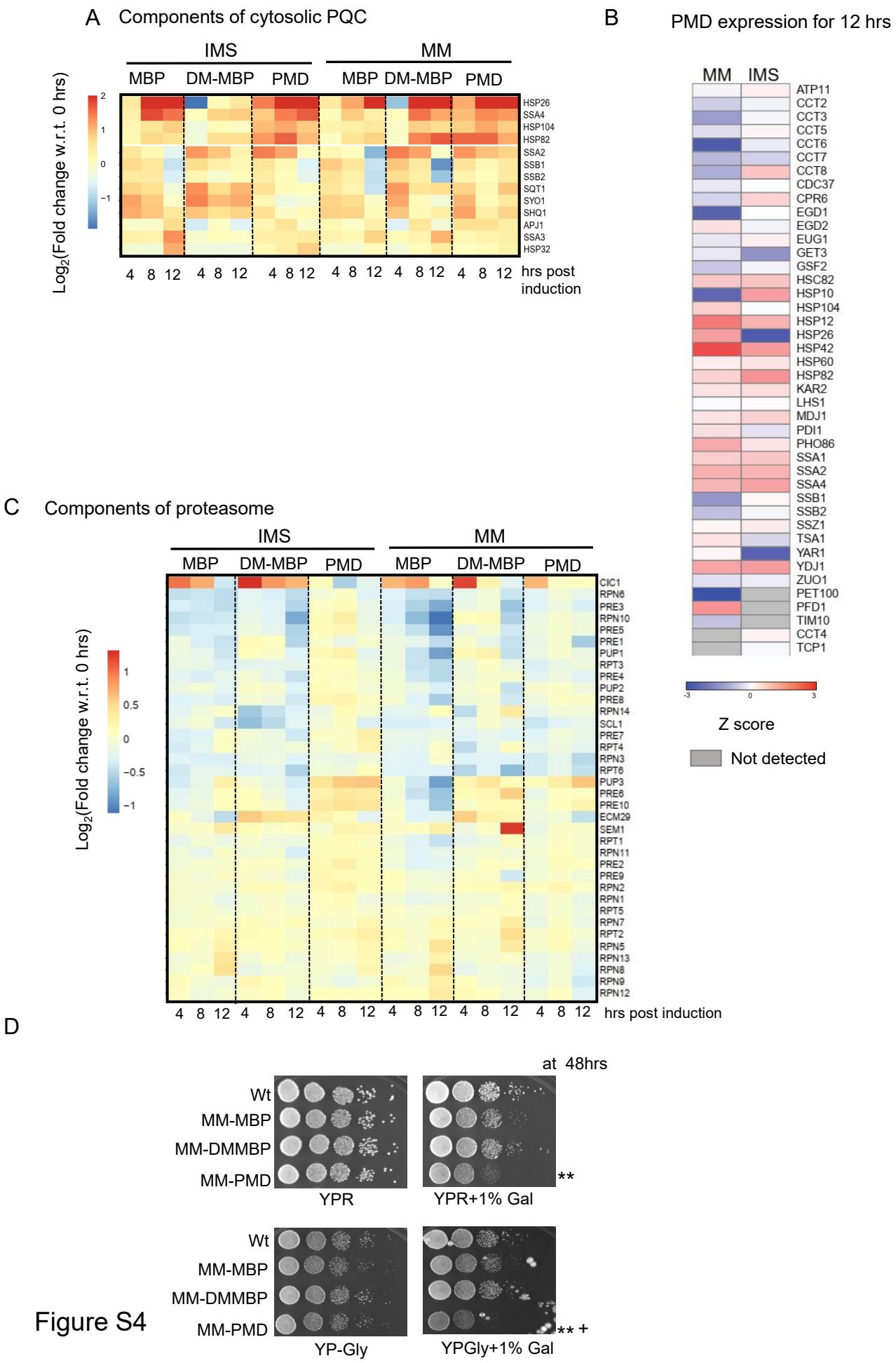
A
Components of cytosolic PQC
IMS
MM
MBP
DM-MBP
PMD
MBP
DM-MBP
PMD
Log2(Fold change w.r.t. 0 hrs)
HSP26
SSA4
HSP104
HSP82
SSA2
SSB1
SSB2
SQT1
SYO1
SHQ1
APJ1
SSA3
HSP32
4 8 12 4 8 12 4 8 12 4 8 12 4 8 12 4 8 12
hrs post induction
B
PMD expression for 12 hrs
MM
IMS
ATP11
CCT2
CCT3
CCT5
CCT6
CCT7
CCT8
CDC37
CPR6
EGD1
EGD2
EUG1
GET3
GSF2
HSC82
HSP10
HSP104
HSP12
HSP26
HSP42
HSP60
HSP82
KAR2
LHS1
MDJ1
PDI1
PHO86
SSA1
SSA2
SSA4
SSB1
SSB2
SSZ1
TSA1
YAR1
YDJ1
ZUO1
PET100
PFD1
TIM10
CCT4
TCP1
Z score
Not detected
C
Components of proteasome
IMS
MM
MBP
DM-MBP
PMD
MBP
DM-MBP
PMD
Log2(Fold change w.r.t. 0 hrs)
CIC1
RPN6
PRE3
RPN10
PRE5
PRE1
PUP1
RPT3
PRE4
PUP2
PRE8
RPN14
SCL1
PRE7
RPT4
RPN3
RPT6
PUP3
PRE6
PRE10
ECM29
SEM1
RPT1
RPN11
PRE2
PRE9
RPN2
RPN1
RPT5
RPN7
RPT2
RPN5
RPN13
RPN8
RPN9
RPN12
4 8 12 4 8 12 4 8 12 4 8 12 4 8 12 4 8 12
hrs post induction
D
at 48hrs
Wt
MM-MBP
MM-DMMBP
MM-PMD
YPR
YPR+1% Gal
**
Wt
MM-MBP
MM-DMMBP
MM-PMD
YP-Gly
YPGly+1% Gal
** +

Figure S4

A

Respiratory chain complex components at protein level after 12 hrs of PMD expression

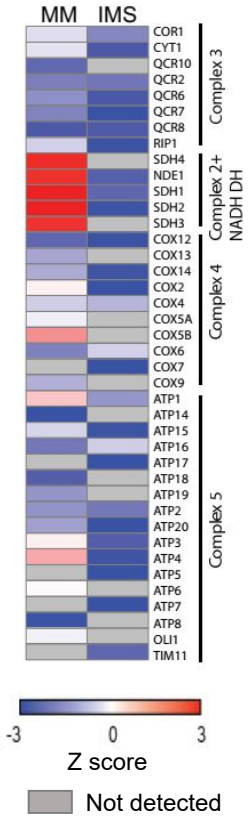

B

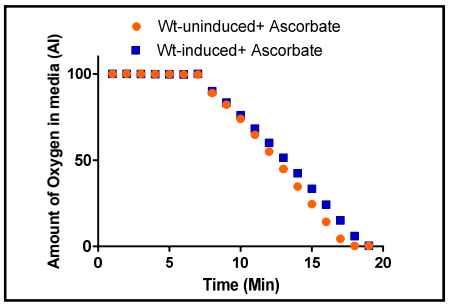

C

Expression of enzymes of Glycolysis by RNA sequencing

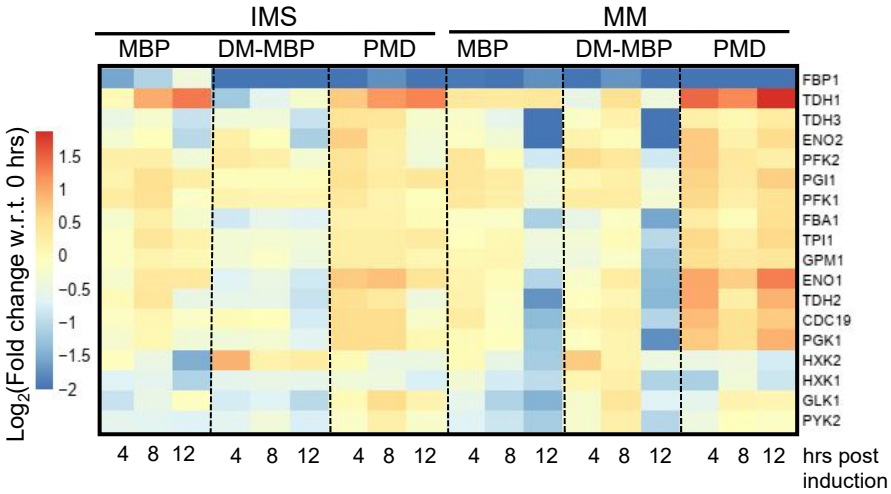

D

Components of Glycolysis at protein level after 12 hrs of PMD expression

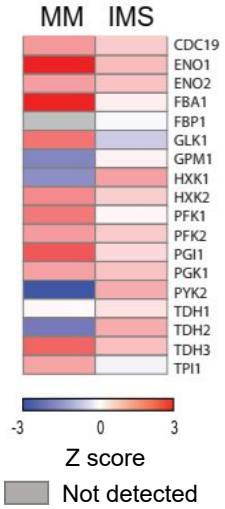

E

Expression of TCA cycle enzymes by RNA sequencing

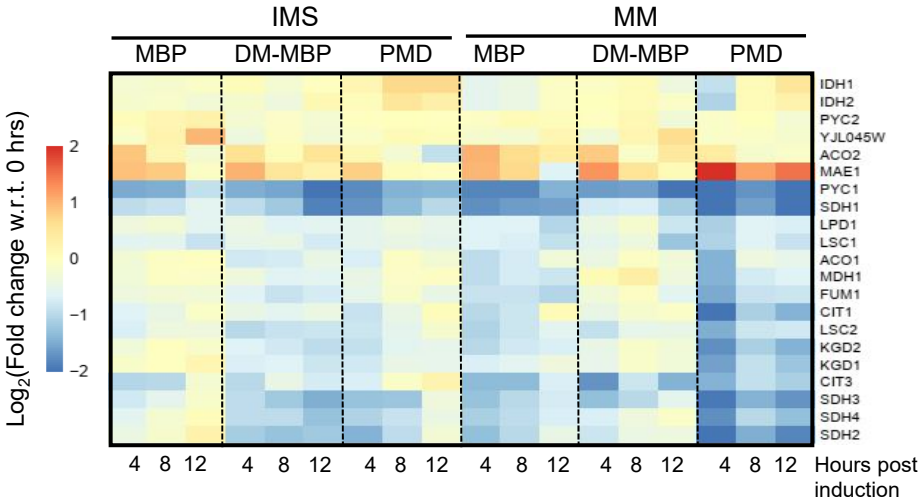

F

Components of TCA cycle at the protein level after 12 hrs of PMD expression

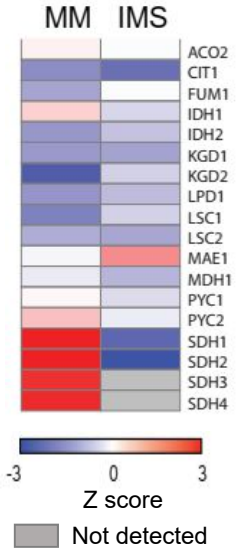

Figure S5

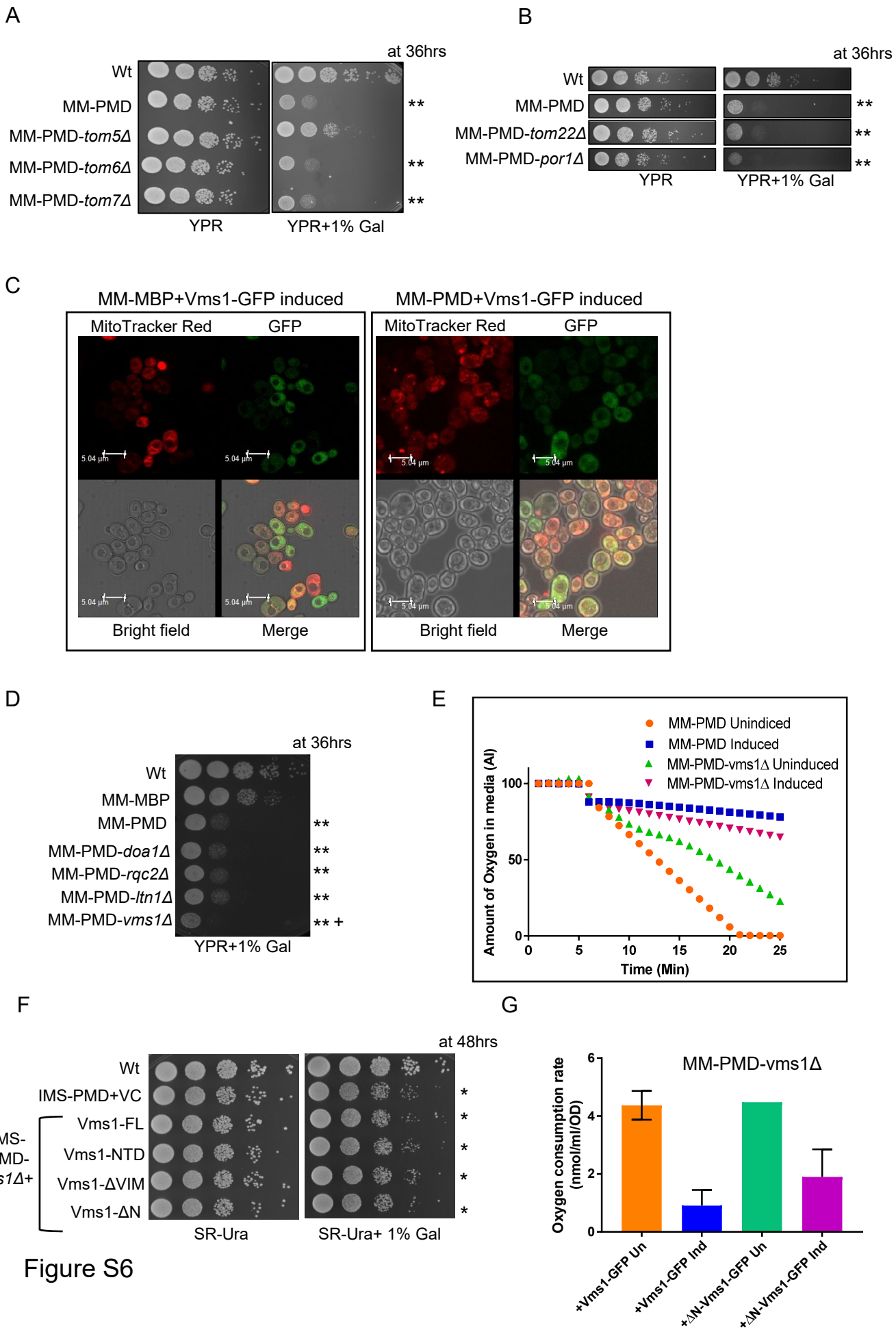
A
at 36hrs
Wt
MM-PMD
MM-PMD-tom5Δ
MM-PMD-tom6Δ
MM-PMD-tom7Δ
**
**
**
YPR
YPR+1% Gal
B
at 36hrs
Wt
MM-PMD
MM-PMD-tom22Δ
MM-PMD-por1Δ
**
**
**
YPR
YPR+1% Gal
C
MM-MBP+Vms1-GFP induced
MM-PMD+Vms1-GFP induced
MitoTracker Red
GFP
Bright field
Merge
MitoTracker Red
GFP
Bright field
Merge
D
at 36hrs
Wt
MM-MBP
MM-PMD
MM-PMD-doa1Δ
MM-PMD-rqc2Δ
MM-PMD-ltn1Δ
MM-PMD-vms1Δ
**
**
**
**
** +
YPR+1% Gal
E
MM-PMD Unindiced
MM-PMD Induced
MM-PMD-vms1Δ Uninduced
MM-PMD-vms1Δ Induced
Amount of Oxygen in media (AI)
100
50
0
0
5
10
15
20
25
Time (Min)
F
at 48hrs
Wt
IMS-PMD+VC
IMS-PMD-vms1Δ+
Vms1-FL
Vms1-NTD
Vms1-ΔVIM
Vms1-ΔN
*
*
*
*
*
SR-Ura
SR-Ura+ 1% Gal
G
MM-PMD-vms1Δ
Oxygen consumption rate (nmol/ml/OD)
6
4
2
0
+Vms1-GFP Un
+Vms1-GFP Ind
+ΔN-Vms1-GFP Un
+ΔN-Vms1-GFP Ind

Figure S6